5-2024

Aldicarb sensitivity is altered in two strains with novel V-ATPase mutations in C. elegans.

Natalie Elizabeth Young
nyoung@bates.edu

Aldicarb sensitivity is altered in two strains with novel V-ATPase mutations in *C. elegans*.

Empirical Honors Thesis

Presented to the Faculty of
the Department of Neuroscience

Bates College

In partial fulfillment of the
Requirement for the degree of the
Bachelor of Arts

By

Natalie Elizabeth Young

Lewiston, Maine
April 1st, 2024

Acknowledgments

I would first like to thank my thesis advisor, Glen Ernstrom, for his commitment helping me construct a written thesis at the highest quality of which I am capable. Prior to his enrollment to his position as visiting assistant professor of Biology and Neuroscience at Bates College, Glen accepted me and my colleague, Adya Agarwal, as his only thesis students. During his transition between institutions, Glen met with me over the summer to educate me on relevant material. We met multiple times in person each week from the start of school through the honors thesis deadline of April 1st, 2024. I thank him greatly for his wisdom, mentorship, unparalleled enthusiasm, dedication, and friendship. Glen offered fantastic support and advice, even through non-thesis related circumstances, such as my veterinary school application process. He truly embraced the role as life mentor, not just a thesis mentor. I will certainly miss seeing his cat, Rosie, in the lab every week.

Secondly, I would like to thank the Bates College Neuroscience department for making this thesis possible. As some may know, the Neuroscience department experienced a significant faculty shortage during 2023. With the largest incoming senior class of neuroscience majors, they feared that they would not be able to offer a thesis experience to these students. However, they made the most out of these difficult circumstances, and decided to offer an honors neuroscience thesis experience to a select group of students. I realize that this was not the easiest decision for the neuroscience faculty to make by any means, which is why I am deeply grateful for the privilege to engage in this thesis experience.

Next, I would like to thank my major advisor and neurobiology professor, Martin Kruse. The education that I received from Professor Kruse regarding fundamental neurobiological mechanisms was integral to my compression of core concepts pertaining to my thesis.

I would also like to thank my animal physiology professor, Ryan Bavis. I experienced my first true scientific writing experience through Professor Bavis's class. His advice on how to write a proper scientific paper has served me well throughout my Bates career, and now, during my senior thesis.

Finally, I would like to thank all of those who have supported me throughout my academic, athletic, and personal growth up until this point. My rock throughout my Bates career were the members of the swim team, and my swim coach, Peter Casares. This community has been my second family, and I know that they have my back both in and out of the pool. Most importantly, I would like to recognize my family and parents, who have played an integral part in every aspect of my successes. Consider this thesis a reflection of the dedication and work of all those who invested in my development, and for whom I am forever grateful.

Table of Contents

Abstract

Synaptic vesicles are individual, uniform packets of neurotransmitters that transmit signals when they fuse to the presynaptic membrane. However, the mechanisms that regulate the quantity of neurotransmitters packaged into synaptic vesicles are not understood. Partially filled vesicles cause impaired signaling (Prado et al. 2006; de Castro et al. 2009; Lima et al. 2010), and vesicles are not maximally filled (Song et al. 1997; Pothos et al. 2000; Wojcik et al. 2004). What controls this set-point? The same vesicular proteins responsible for neurotransmitter loading may also determine fusion competence. Prior work has ruled out neurotransmitter quantity as a prerequisite for vesicle fusion (Ernstrom personal communication; Parsons et al. 1999), but has instead suggested a role of the pH gradient generated by the V-ATPase proton pump (Ernstrom personal communication; Rost et al. 2015). If a vesicle pH threshold is a determinant for vesicle release, then we expected to recover genetic variants where V-ATPase activity is correlated with vesicle fusion. To test this model, we screened candidate V-ATPase mutants in genetically tractable nematodes, *Caenorhabditis elegans,* for their sensitivity to the nematicide organophosphate, aldicarb. Aldicarb causes toxic, paralyzing accumulation of neurotransmitters in the neuromuscular junction between neurons and muscles. Animals that are resistant to the paralyzing effects of aldicarb typically have a defect in neurotransmitter release, while hypersensitive animals typically have abnormally high rates of neurotransmitter release (Mahoney et al. 2006). This thesis will present the quantitative analysis of V-ATPase mutants where the molecular mutations have been mapped, but the aldicarb sensitivity phenotypes have not been characterized. We identified resistance and hypersensitivity in two mutant strains respectively, suggesting a possible role of V-ATPase proton pump acidification in vesicle fusion competency.

Introduction

Chemical neuronal synaptic neurotransmission is mediated by the electrically stimulated release of neurotransmitters. This form of neurotransmission relies on individual, uniform quantities of neurotransmitters into synaptic vesicles (Südof, 2004). If these synaptic vesicles are not adequately filled, this causes dysfunction such as impaired locomotion (Prado et al. 2006; McIntire et al. 1997), impaired cognition (Prado et al. 2006; de Castro et al. 2009), impaired memory (Prado et al. 2006). Neurotransmitter loading and release appears to be regulated. If vesicles are partially filled, impaired signaling results, which affects normal behavior (Prado et al. 2006; de Castro et al. 2009; Lima et al. 2010). Prado et al. 2006 found that VAChT homozygous mice (where VAChT is a deficiency that alters synaptic vesicle filling) exhibited significant decreases in motor learning and in their ability to perform sustained physical activity. Additional work demonstrates vesicles are not maximally filled (Song et al. 1997; Pothos et al. 2000; Wojcik et al. 2004). Although the fusion of uniform packets at presynaptic terminals is well known, a long standing question of what determines quantal size is not known. An emerging hypothesis is that the enzymes involved in loading neurotransmitters into vesicles also serve in a quality control checkpoint to ensure only vesicles that are loaded can fuse (Rost et al. 2015; Bodzeta et al. 2017; Ernstrom personal communication). To begin we review key aspects of the synaptic vesicle cycle.

Chemical Synaptic Transmission

Chemical synaptic transmission depends on the regulated exocytosis of synaptic vesicles loaded with neurotransmitters. The process of chemical synaptic transmission is outlined as follows **(Figure 1**) (Levitan and Kaczmarek, 2015):

1. Loading is the secondary-active transport of neurotransmitters in synaptic vesicles.
2. Docking is the loose tethering of vesicles to plasma membrane-associated proteins.
3. Priming is the tight association of the vesicle with the plasma membrane in preparation for fusion.
4. Calcium-sensing is the enhancement of the probability of fusion caused by an influx of calcium through voltage-gated calcium channels.
5. Fusion is the merger of the vesicle membrane to the plasma membrane.
6. Recycling is the reformation of synaptic vesicles by the pinching off of a portion of plasma membrane from the synaptic terminal.

Once vesicles have been loaded and loosely docked onto the terminal plasma membrane, they are ready to proceed into the priming phase. Priming involves a tight intertwinement of soluble N-ethylmaleimide sensitive factor attachment protein receptors (SNARE-complex proteins), which tether synaptic vesicles to the plasma membrane in preparation for fusion (Levitan and Kaczmarek, 2015). Terminal depolarization triggers activation of voltage-gated calcium channels and the subsequent transient influx of calcium ions. Calcium sensing is achieved by a protein called synaptotagmin, which will kickstart the fusion of the vesicular membrane with the terminal plasma membrane in response to calcium influx (Jahn and Südhof, 1999). Promptly following the fusion event, neurotransmitters are exocytosed into the synaptic

cleft, where they are free to evoke their effects on the postsynaptic terminal by binding cognate receptors.

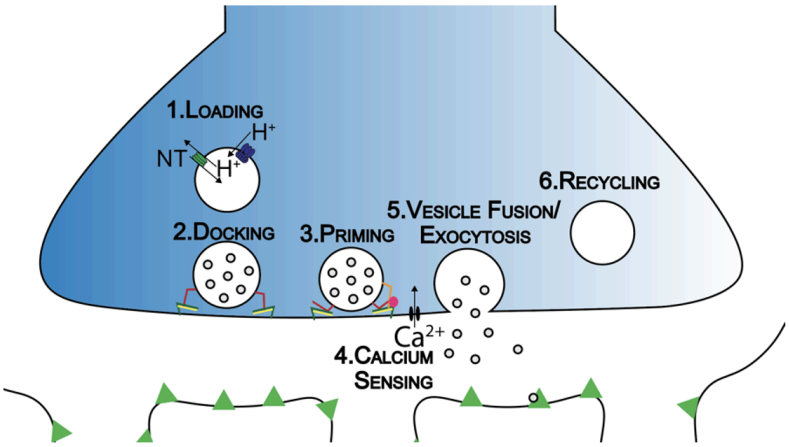

Figure 1. The process of synaptic transmission.
A chronological depiction of (**1**) the loading phase involving secondary active transport of neurotransmitters, (**2**) the docking phase involving the loose association vesicle with the SNARE proteins, (**3**) the priming phase involving the close association of a vesicle with the SNARE proteins, (**4**) vesicle fusion and exocytosis of neurotransmitter to the synaptic cleft and its subsequent binding to postsynaptic receptors, and (**5**) vesicular recycling.

Neuromuscular junctions have been a model to investigate the molecular mechanisms of neurotransmitter release. At vertebrate and nematode neuromuscular junctions, the excitatory neurotransmitter acetylcholine is released from motor neurons (Changeux, 2020; Levitan and Kaczmarek, 2015). For our purposes, the class of ACh receptor at skeletal muscles is nicotinic. Nicotinic receptors require the binding of ACh, which triggers ligand-gated ion channels to open, allowing for the diffusion of ions (typically sodium) from the synaptic cleft into the skeletal muscle cell. Following sufficient stimulation, and depolarization of the muscle cell, muscle contraction will ensue (Levitan and Kaczmarek, 2015).

Terminating neurotransmitter signaling requires either enzyme transmitter or reuptake transporters on the presynaptic terminal. The most common form of neurotransmitter inactivation involves neurotransmitter specific transporters located in the membrane of the presynaptic terminal (Hyman, 2006). However, in the case of ACh, inactivation is achieved by degradation from enzymes located in the synaptic cleft. Neurotransmitter derivatives are reabsorbed by

transporter molecules located in the plasma membrane of the presynaptic terminal (Iversen, 2006). Once reintroduced to the presynaptic terminal, these derivatives can then be recycled for further signaling use (Hyman, 2006).

This thesis will focus on mechanisms of synaptic vesicle loading with respect to engagement with the "fusion machinery," the proteins that dock, prime, and catalyze membrane fusion.

Vesicle Loading

Vesicle loading is the process by which neurotransmitters are packaged into synaptic vesicles during the process of synaptic transmission. Neurotransmitters are loaded in a multi-step process called secondary-active transport. This process involves the transport of neurotransmitters against their electrochemical gradient, coupled to the facilitated diffusion of ions along their electrochemical gradient (Schetcher, 1986). Thus, the energy requirement to move neurotransmitters into a vesicle is met by the electrochemical potential from actively pumping ions first into the vesicle, and then allowing them to passively diffuse out.

The proteins responsible for translocating neurotransmitters into synaptic vesicles are vesicular neurotransmitter transporters. There are four classes of vesicular transporters: vesicular monoamine transporter (VMAT), vesicular GABA transporter (VGAT), vesicular glutamate transporter (VGLUT), and vesicular acetylcholine (ACh) transporter (VAChT) (Levitan and Kaczmarek, 2015). VMAT is responsible for loading serotonin, dopamine, epinephrine, and norepinephrine. Alternatively, VGAT is responsible for loading the zwitterionic neurotransmitter, GABA (Omote and Moriyama, 2013; Anne and Gasnier, 2014). Systems involving the loading

of zwitterionic neurotransmitters are dependent on both the membrane potential and vesicle pH (Takamori, 2016; Anne and Gasnier, 2014). VGLUT is responsible for loading the anionic neurotransmitter, glutamate (Anne and Gasnier, 2014). The exchange of anionic neurotransmitters is dependent on the membrane potential, whereas the loading of the cationic neurotransmitter, ACh, achieved by VAChT, is thought to be strictly dependent on vesicle pH (Takamori, 2016). Regardless of neurotransmitter and transporter type, it has been observed that the amount of neurotransmitters loaded into each individual vesicle are relatively uniform in size (Fatt and Katz, 1951; del Castillo and Katz, 1954; Edwards, 2007).

This first evidence of this discovery was documented in 1952 by Bernard Katz and Paul Fatt who observed constant subthreshold electrical activity in the neuromuscular junctions between neurons and frog sartorius muscles, even in the absence of a stimuli. They described these electrical events as small, intermittent, and spontaneous. The nature of these subthreshold electrical events were similar to the end plate potentials (e.p.p) produced by strong nerve impulses, with the only notable difference being their amplitude (0.5mV compared to > 50mV). Fatt and Katz named these small, spontaneous events mini end plate potentials (m.e.p.p). In order to observe the relationship between these e.p.p's and m.e.p.p's, Fatt and Katz measured the electrical activity in frog neuromuscular junctions from strong stimulation following the iontophoretic application of curare (which is a drug that suppresses the response of the postsynaptic neuron to ACh). They observed that the discrete, all-or-none behavior exhibited by artificially induced ACh potentials of standard size and time course, could be significantly altered following the application of curare. That is, they were able to continually reduce the size of ACh potentials below a detectable level, and they were able to smoothly alter the time course

of the associated electrical events. They suspected that m.e.p.p's were caused by leakage of ACh from the nerve ending, however, more convincing evidence was needed to answer this question.

In 1954, del Castillo and Katz continued the investigation into the relationship between e.p.p's and m.e.p.p's. They followed similar methods to the experiment conducted by Katz and Fatt in 1952, but this time, they recorded the amplitudes of all ACh potentials and plotted them on a histogram for comparison. They observed that relative size and time course of electrical events followed a similar distribution, which is outlined by Poisson's law. Furthermore, they were able to determine the amplitudes of subsequent potentials in a series from largest (> 50mV e.p.p) to smallest (0.5mV m.e.p.p) were proportional. That is, each class of e.p.p amplitudes was divisible by the smallest e.p.p unit (or m.e.p.p). They reasoned that if the uniform size of multiple m.e.p.p can sum to approximate the amplitude an e.p.p., then the m.e.p.p must represent the basic unit of response.

Following years of additional work, this evidence ultimately led Bernard Katz to formulate his famous quantal theory, which states that:

1. Neurotransmitters are released in fixed amounts as discrete packets (quanta).
2. m.e.p.p's represent the electrical potential induced by release of neurotransmitters.
3. Quanta are released in response to the arrival of a single action potential.
4. Variability in the size of e.p.p's is a result of the number of quanta released (Katz, 1969).

At the time, Katz was not aware that synaptic vesicles were the cellular unit that he referred to as "quanta." However, these studies conducted by Katz and colleagues led to subsequent studies, ultimately detailing the vesicle as the synaptic packages containing neurotransmitters. These following studies included Ulf Von Euler's freeze-etch preparations of

bovine splenic nerve granules and guinea-pig vas deferens adrenergic nerve terminal, and Julius Axelrod's electron micrographs of cat pineal glands (Axelrod, 1981; Euler, 1971).

Fusion Checkpoint

One question that emerged following the proposal of the quantal hypothesis was what regulates quantal size? That is, what qualities of synaptic transmission regulate the uniform amount of neurotransmitters packaged into synaptic vesicles, and what determines their readiness for priming and calcium sensing? Two major models were derived in response to these questions. The first suggested that synaptic vesicles directly detect neurotransmitter levels to ensure they are properly loaded. In other words, the neurotransmitter levels themselves serve as a prerequisite for vesicle priming and fusion. If this were true, one might expect that partial loss-of-function mutations in the neurotransmitter transporters would cause normally filled vesicles to fuse at a slower rate. However, if some other quality of the synaptic vesicles served as a proxy for neurotransmitter levels, one might expect that this same partial loss-of-function mutation in neurotransmitter transporters would cause partially filled vesicles to fuse at normal frequency. A study conducted by Parsons et al. in 1999 applied the pharmacological treatment of 5mM vesamicol to inhibit the vesicular ACh transporter in snake muscles. They were able to quantify quantal content using FM dye experiments, which is a type of live imaging experiment that labels recycling vesicles. They found that the rate of endo- and exocytosis persisted at a consistent, high rate throughout the duration of their experiment (~120 minutes), while the miniature end plate current (MEPC) amplitude declined. Thus, underfilled synaptic vesicles continued to dock and exocytose at a consistent rate. Similar results have been replicated in mice deficient in VMAT and VGLUT (Croft et al. 2005; Wojcik et al. 2004). Stronger evidence of

synaptic vesicle overstuffing has been reported as a result of vesicular transporter overexpression (Pothos et al. 2000). These results are not consistent with the first model suggesting that neurotransmitter levels act as a checkpoint, either inhibiting or permitting docked vesicles to proceed through the later stages of neurotransmission. Thus, there must be some other indirect measurement that ensures vesicles are properly filled.

The second major model that attempts to answer the fusion readiness question is the pH model, which suggests that vesicles indirectly measure neurotransmitter quantity by detecting the level of vesicle acidification. Results consistent with this hypothesis would fulfill the predictions that changes in vesicle pH would result in normally sized quanta that fuse at abnormal frequencies. If acid does not regulate quantal content, there would be no effect of pH on the rate of vesicle fusion. Ernstrom et al. (unpublished) and Bodzeta et al. (2017) attached a pH sensitive green fluorescent protein, pHluorin (Miesenböck et al. 1998) to synaptobrevin (Sankaranarayanan et al. 2000) in order to determine the level of acidification in mutants deficient in proton-pumping machinery. They observed lower levels and frequency of acidification (indicated by brighter fluorescence) in mutants compared to wild-type animals. They also found evidence that the gaussian distribution of quantal size in these pH deficient mutants was right shifted, indicating that some vesicles may contain a higher density of neurotransmitters than normal. Perhaps vesicles were held longer at this loading checkpoint, allowing for more neurotransmitters to be packaged than normal. This current evidence is more consistent with the second model suggesting that pH acts as a checkpoint for vesicle fusion. The molecular machinery responsible for vesicle acidification is achieved by a biologically conserved vesicular trans-membrane protein, known as the vacuolar proton pump (V-ATPase) (Bowman et al. 1992; Forgac, 1997).

V-ATPase Proton Pump

The first step in the vesicular loading process is achieved by the V-ATPase proton pump. The V-ATPase is a multi-subunit complex that is composed of two sectors: the cytoplasmic V_1 sector which hydrolyzes ATP, and the transmembrane V_o sector which translocates protons across the membrane (**Figure 2)** (Bowman et al.1992). The V_1 sector is composed of eight different subunits. This includes a hexamer alternating between A and B subunits, a central rotor axle consisting of subunits D and F, subunits G and E acting as peripheral stators, and regulatory subunits C and H. On the other hand, the V_o sector is composed of six different subunits which include subunits a, b, c, c^I, c^{II}, and e (Bowman et al. 1992; Forgac, 1997). These various subunits composing the V_1 and V_o sectors of the V-ATPase exist in different isoforms. The B and H subunits of the V_1 sector have been found to have two isoforms, whereas the a and c subunits of the V_o sector have been found to have four and three isoforms respectively (Ernstrom et al.

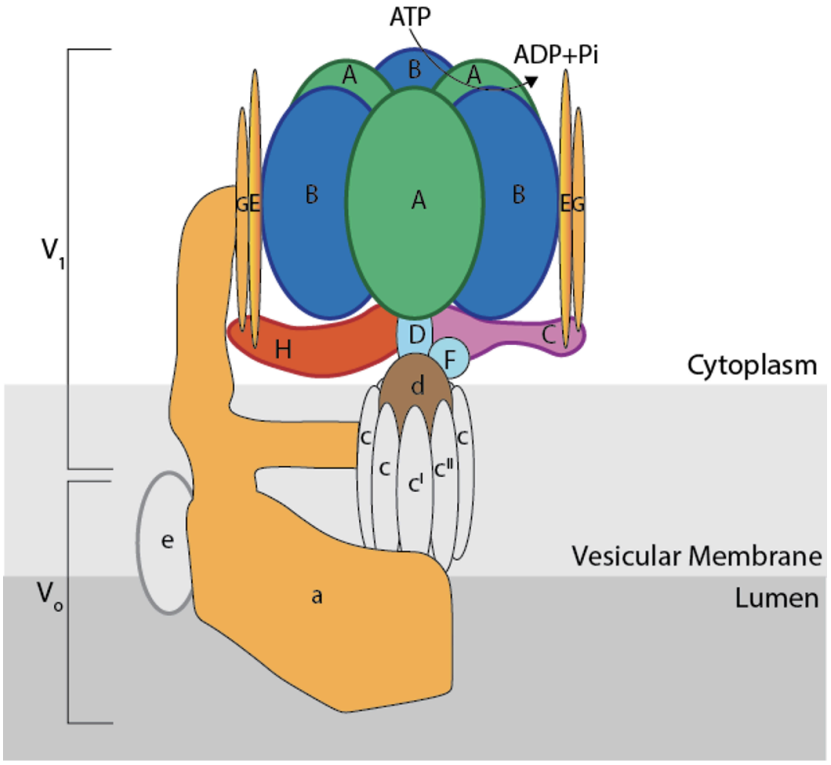

Figure 2. The V-ATPase is composed of the cytoplasmic V_1 sector, including subunits, A, B, C, D, E, F, G, and H, and the transmembrane V_0 sectors including subunits a, b, c, c^I, c^{II}, and e.

2012). Localization of these isoforms are generally expressed in different cell types, giving rise to different varieties of V-ATPases that function on similar machinery, but perform separate roles in different contexts (Toei et al. 2010; Forgac, 2007). For instance, the B1 subunit of the V_o sector has been localized to epithelial cells in the inner ear, kidney, and vas deferens, where it is responsible for translocating protons into the extracellular space (Brown et al. 2009). Alternatively, the B2 isoform of the V_o sector is more readily found on intracellular organelle membranes, such as synaptic vesicles (Brown et al. 2009). In fact, most (if not all) cells require a variation of transmembrane V-ATPases on their organelles, including: lysosomes, endosomes, vacuoles, golgi, and synaptic vesicles - in order to acidify these compartments, which allows for their function and proper storage of distinct intracellular molecules (Forgac, 2007).

With respect to V-ATPases localized to synaptic vesicles, the V_1 sector ultimately fulfills the initial energy requirement for secondary-active transport and vesicle acidification. This energy provided by ATP hydrolyzation ultimately drives the V_o sector central rotor component, which generates an electrochemical gradient by shuttling protons against their concentration gradient into synaptic vesicles (Beyenbach and Wieczorek, 2006). Various studies have suggested an optimal synaptic vesicle pH ≈ 5.2 - 5.5 following acidification, and an average extracellular medium pH ≈ 7.25 (Ahdut-Hacohen et al. 2004). The energy from this electrochemical gradient can later be harnessed to drive neurotransmitters into synaptic vesicles via specialized transporters, to complete the process of secondary active transport (Beyenbach and Wieczorek, 2006). Besides energizing synaptic vesicles for neurotransmitter loading, some studies have suggested additional roles of vesicular V-ATPases. It is currently debated whether V-ATPases aid in quantal release by serving as a fusion catalyst (El Far and Seagar, 2011; Jahn and Südhof, 1999; Hiesinger et al. 2005; Zhou et al. 2000) or if their role of acidifying synaptic

vesicles acts as a checkpoint prior to priming (Rost et al. 2015; Ungermann et al. 1999; Marshansky, 2007).

V-ATPase V_o as a Fusion Catalyst

The membrane anchored V_o sector may catalyze a late step in vesicle fusion to the plasma membrane. This is called the fusogen model. The fusogen model suggests that both the V_1 and V_o sectors are responsible for vesicle acidification which is required for the secondary active transport of neurotransmitters, however, only the V_o sector is able to associate with the plasma membrane and is responsible for quantal release (El Far and Seagar, 2011; Jahn and Südhof, 1999). Some more radical hypotheses suggest that this association is achieved by the dissociation of the V_o sector from the V_1 (Lu et al. 2007; Stevens and Forgac, 1997; El Far and Seagar, 2011), however, not all who support this hypothesis align with this view. Evidence supporting the fusogen model is outlined below.

In a study conducted by Morel et al. in 2003, researchers cloned a V-ATPase a1 isoform, *Torpedo marmorata*, which is localized primarily to nerve endings. They performed immunogold detection of the V-ATPase V_o sector c and a subunits in freeze fractured nerve endings. They found that c subunits, but not the a subunits, were localized to the presynaptic membrane during and following fusion. They suggested that the negative results for the a subunit could have been caused by masking of the epitope by the PT/C replica. From these results, they concluded that the V_o sector of the V-ATPase associates with both the plasma membrane and synaptic vesicles as a result of fusion catalysis. Interestingly, they also found evidence that the A and B subunits of the V_1 sector associate with the terminal plasma membrane, which conflicts with the hypothesis

that the V_1 sector dissociates from the plasma membrane during fusion. Additionally, this experiment did not observe direct interactions between t-SNARE proteins and the V-ATPase, nor did it acknowledge that a portion of these positive results could have been collapsed vesicles on the plasma membrane prior to recycling.

Another study that adopted this genetic approach in favor of investigating the fusogen model is one performed by Hiesinger et al. in 2005, who studied Drosophila with loss-of-function *vha100-1* mutations affecting the V_o sector of the V-ATPase proton pump. From their results, the authors reported a late step exocytotic role of the V_o sector, in favor of the fusogen model. Interestingly, the authors also reported a significantly reduced frequency of mEPSPs (mini excitatory postsynaptic potentials) at the neuromuscular junction in *vha100-1* mutants compared to the control. They found no significant difference between the amplitude of mEPSCs of the *vha100-1* mutants and the control, which seems to suggest a relationship between vesicle acidification and rate of quantal release. It appears that some of the evidence from this study conflicts with the authors' overall conclusions.

Other studies have taken an alternative route in studying this phenomenon by using the pharmacological application of bafilomycin (Baf), a V-ATPase c subunit inhibitor (Mauvezin and Neufeld, 2015). In a study conducted by Zhou et al. in 2000, FM 1-43 data showed that the blockage of proton pumping with the application of Baf resulted in a reduction of both the amplitude and frequency of GABAergic and glutamatergic MEPSP's in rat hippocampal neurons. This data suggests that reduced function of proton pumping results in minor decreases in both quantal size and rate of fusion. These authors suggested that the probability of exocytosis appears to be entirely independent from the filled state of the vesicle. In their methods, the authors noted that rat hippocampal neurons of the CA1 and CA3 regions were cultured out of

their typical context (the hippocampus). Additionally, the cultured rat hippocampal neurons were incubated with Baf over a long time scale (1 hour), prior to recording, which could have convoluted the results from off target effects. Perhaps the culture should have been treated on an acute time scale in order to observe the immediate effects of Baf on vesicle fusion frequency and quantal size.

Despite the evidence in favor of the fusogen model, it appears that most of the results supporting this model are inconsistent or indirect measurements prone to misinterpretation or experimental errors. It is still unclear to what extent (if any) the V-ATPase interacts with plasma membrane associated fusion proteins, however, there is minimal evidence disproving the role of acidification as a fusion checkpoint.

Vesicle Acidification State as a Requirement for Fusion

Several lines of evidence from neuronal and non-neuronal systems are consistent with the hypothesis that acidification is required for vesicle fusion in trafficking pathways (otherwise known as the pH model). First, bafilomycin blocks i*n vitro* yeast vacuole fusion and trans-SNARE pairing (Ungermann et al. 1999). Second, early to late endosome trafficking in renal endocytic vesicles is also blocked by bafilomycin (Marshansky, 2007). Third, optogenetic restoration of a proton gradient can drive the fusion of vesicles independent of V-ATPase activity, which is evident from data indicating that partially filled vesicles exhibit a lower release probability (Rost et al. 2015; M.T. Palfreyman and E.M. Jorgensen personal communication). Additionally, this evidence may be suggestive of a relationship between rate of vesicle loading

and vesicle fusion probability (supportive of the pH model), which is a function of vesicle acidification and the V_1 sector.

A challenge within this topic of study is the reconciliation of conflicting observations regarding the precise role of the V-ATPase at neuronal synapses. One approach to define the necessity of different V-ATPase sectors in the process of synaptic transmission. Although many studies have focused primarily on the associative properties of the membrane rotor V_o complex, few studies have investigated the requirement of the catalytic V_1 subunit activity for membrane fusion. The alternative route may provide more detailed information regarding the role of vesicle acidification in the requirement for fusion.

Caenorhabditis elegans as a Model Organism

The optimal model organism to study the effects of V_1 sector induced changes in vesicle pH on quantal release in vitro, is *Caenorhabditis elegans*. *C. elegans*, or the nematode, is a well characterized organism complimented by a wide base of scientific literature. Each of the nematode's 302 nerve cells, 5000 chemical synapses, 2000 neuromuscular junctions, and 600 gap junctions have been identified, named, and mapped using reconstructions of electron micrographs of serial sections (White et al. 1984). This fully characterized genome offers significant benefits including a comprehensive understanding of the interaction between genes, the molecules they code for, observed phenotypes for molecular and genetic studies, heightened validity, and increased experimental reproducibility.

C. elegans exist as self fertilizing hermaphrodites (females) and males, which allows for ease of genetic manipulation (Corsi et al. 2015). "Selfing" follows Mendelian segregation rules,

such that heterozygous parents will produce an offspring ratio of 1:2:1. Because hermaphrodites cannot mate with other hermaphrodites (rather they temporarily produce their own sperm prior to oocytes in order to self fertilize), this means that homozygous mutants are more easily produced and maintained in a laboratory setting (Brenner, 1974).

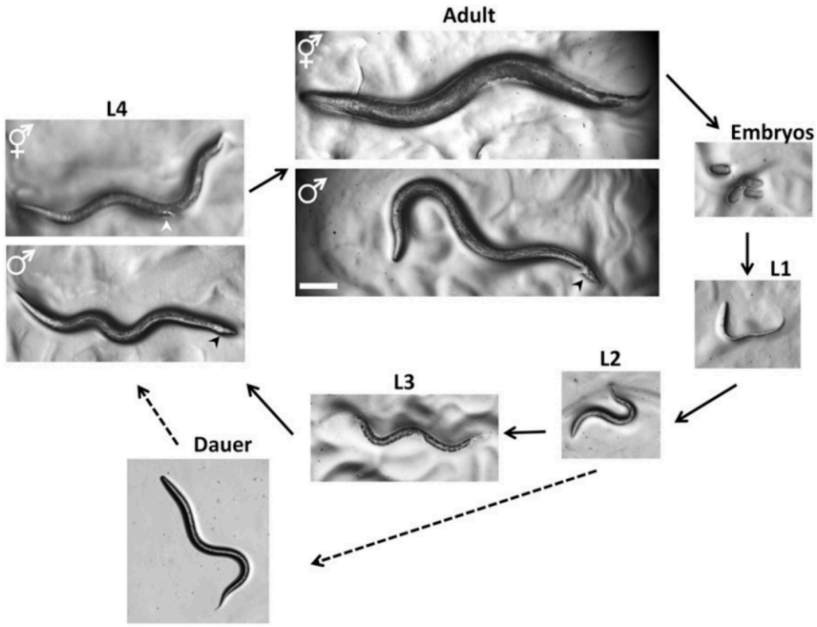

Figure 3. The life cycle of *C. elegans.*

C. elegans development begins at the embryonic stage, where they progressively increase in size throughout each of the larval stages (L1, L2, L3, and L4). By the L4 stage, hermaphrodites can be distinguished from males by their developing vulva (identified by the white arrowhead) and tapered tail. Males have a wider tail (identified by the black arrowhead), which will eventually develop into a fan shape by adulthood. Adult hermaphrodites are thicker and have a more tapered tail than adult males, who are skinnier and have a fan-shaped tail. Dauer larvae that diverge after the L2 stage are skinnier than worms at any of the other larval stages. This figure was adapted from Corsi et al. 2015.

Another benefit of *C. elegans* is their rapid development period. Growth of wild-type animals occurs in three days from embryo to adult at room temperature. There are four larval stages from the time they are conceived as embryos to adulthood (**Figure 3**) (Corsi et al. 2015). Embryogenesis lasts approximately ~16 hours when kept at 20˚C. From embryos, they will proceed into their first larval stage L1, which also lasts 16 hours. Larval stages L2 - L4 each last approximately twelve hours (Raizen et al. 2008). However, prior to proceeding from larval stage L2 to L3, *C. elegans* may arrest development and diverge into "Dauer larvae" under restricted food and growth conditions. These larvae are sterile and their cuticle is more resistant to chemicals and environmental stressors. However, *C. elegans* adults exhibit an absorbent cuticle, which makes them optimal candidates for drug assays on solid agar plates (Wright, 1987). Dauer larvae can be maintained for months and will resume growth in larval stage L4 once proper food and growth conditions are provided (Golden and Riddle, 1984). After stage L4, *C. elegans* will molt their cuticle layer and become adults. Approximately 2 - 3 days after molting, hermaphrodites will be capable of producing progeny (Corsi et al. 2015). In adulthood, *C. elegans* reach a maximum diameter of about 1mm (Corsi et al. 2015). In addition, *C. elegans* neurons express a wide variety of ion channels (including a large number of potassium channels) and they utilize many common neurotransmitters (including ACh, glutamate, GABA, dopamine, and serotonin) (Starich et al. 2001; Hobert, 2013). In fact the molecular identity of the genes that encode vesicular transporters for the neurotransmitters ACh and GABA were discovered in *C. elegans* (McIntire et al. 1997; Rand et al. 2000). The *C. elegans* nematode has become one of the most frequently used models to study evolutionarily conserved genes (Lee et al. 2010).

C. elegans are easy to grow in the laboratory. Due to their small size, low maintenance expense, invariant cell number, quick generation time, and non harmful nature to humans (they

are unable to survive at human body temperature), *C. elegans* can be grown on agar plates with a lawn of *Escherichia coli*. At bare minimum, they require nothing more than a dissecting microscope in order to be observed. Self-fertilizing hermaphrodites are easily propagated by translocating fertile adults to fresh plates with more bacterial food. Starved, dauer larvae can enter a long-lived developmental stage where such individuals can survive for six months at 15˚C (Corsi et al. 2015). For long term storing, they are best if kept at a temperature between 12˚ to 15˚C, and their Q_{10} is approximately ~2 (which means that for every 10˚C increase in temperature, their growth rate increases by a factor of two). Further, strains can be frozen and stored for years at -80˚C. They can be revived following a thawing procedure (Sulston and Hodgkin, 1988). However, *C. elegans* may become sterile if kept at temperatures of 25˚C and above (Corsi et al. 2015). Shorter exposure to these higher temperatures through heat shock treatments can increase the probability of producing males. These nematodes also exhibit an optically clear cuticle, which facilitates the visualization of tagged proteins for studying optogenetic physiology (Corsi et al. 2015). In addition, electrophysiological methods are established, which are the same methods that have been used to quantify neurotransmitter release directly in other animals (Francis and Maricq, 2006).

Despite the advantages of using the nematode as a model organism, they do have some limitations. Their small size can sometimes be a drawback because it makes experimental manipulation of specific tissues difficult. For example, electrophysiological experiments of single cells are difficult, demanding, and time intensive (however still possible). Lastly, although the *C. elegans* community has a wide base of shared research, some biochemical approaches in this model organism lag behind the genetic approaches (Corsi et al. 2015). Regardless, the *C. elegans* nematode provides an optimal model system for studying biologically conserved,

fundamental signaling processes with ease. For this study we did not perform electrophysiological analysis but we leveraged an *in vivo* population assay that correlates well with electrophysiological analysis.

Experimental Design

Synaptic transmission in *C. elegans* can easily be studied through a pharmacological approach using different assays. The most common assay used is aldicarb (2-methyl-2-(methylthio)propionaldehyde o-(methylcarbamoyl)-oxime), which is a reversible acetylcholinesterase inhibitor (Mahoney et al. 2006). Acetylcholinesterase is an enzyme located in the neuromuscular junction which causes rapid hydrolysis of ACh (Miller et al. 1996). Thus, aldicarb causes an accumulation of ACh in the synaptic cleft during muscle contraction, which will induce a state of fused tetanus, paralysis, and even death in affected *C. elegans*. Due to variation between individuals or genetic mutations, worms can have altered sensitivity to aldicarb. *C. elegans* that are resistant to acetylcholinesterase inhibitors are called "Ric" mutants, whereas those hypersensitive to acetylcholinesterase inhibitors are called "Hic" mutants (Mahoney et al. 2006).

An alternative assay that can be used to study synaptic transmission in *C.elegans* is levamisole, which acts as a cholinergic agonist (directly activates ACh receptors on the postsynaptic terminal) (Mahoney et al. 2006). Levamisole and aldicarb can be used with the same methodologies, however, they test different effects. Because levamisole acts on ACh receptors in the synaptic cleft, it is only effective for studying genes that affect the postsynaptic compartment. In addition, levamisole may not be able to detect all postsynaptic effects because

C. elegans body wall muscles express some levamisole-resistant ACh receptors. In order to detect genes that affect the presynaptic cell, aldicarb should be used. However, it is not possible to establish with certainty whether mutated genes affect the pre- or postsynaptic cells when treated with aldicarb, and thus additional tests should be conducted to establish which side of the synapse is affected. If a worm is resistant to aldicarb and sensitive to levamisole, the mutated gene likely operates in the presynaptic compartment (Mahoney et al. 2006). This is also true for worms exhibiting hypersensitivity to aldicarb, and resistance to levamisole. However, if worms are hypersensitive to both aldicarb and levamisole, or resistant to both aldicarb and levamisole, the gene may operate in the postsynaptic cell (Mahoney et al. 2006). My study focused on the application of aldicarb, while my colleague, Adya Agarwall, studied the postsynaptic effects with levamisole.

There are currently three established protocols for analyzing synaptic transmission in *C. elegans*: the dose response to aldicarb assay, the population growth rate assay, and the time course of aldicarb paralysis assay (a.k.a population survival assay). For the applicable protocols, a worm qualifies as paralyzed when they display no movement in response to being gently prodded three times with a platinum wire. A worm can also qualify as paralyzed with cessation of pharyngeal pumping (Mahoney et al. 2006; Alfonso et al. 1993).

The dose response to aldicarb assay begins when *C. elegans* are incubated with various concentrations of aldicarb (or levamisole) for 5 - 6 hours, and the ratio of worms still moving is recorded as a function of the concentration of the selected assay. This protocol generally requires a large number of age matched worms for each strain being tested, and it takes a longer time period to complete (10 hours) (Mahoney et al. 2006).

Another alternative, the population growth rate assay, is a good choice for those concerned about possible biases related to the paralysis scoring method required for the other two protocols. This protocol requires that *C. elegans* nematodes are grown in the presence of various doses of aldicarb. Once fully matured, the total number of progeny for each of the different aldicarb doses is compared with the number of progeny produced when grown in the absence of aldicarb (or the alternative assay). This experiment is relatively quick to conduct, and the results have been shown to correlate well with electrophysiological results. However, the readout (production of progeny) is not directly correlated to the effects of the assay on synaptic transmission (Mahoney et al. 2006).

The final protocol, and that which is most closely linked to the action of the chosen assay, is the time course of aldicarb paralysis assay. Various studies have shown that the results produced from this experiment correlate well with data obtained from electrophysiological assays of synaptic efficacy (Koushika et al. 2001; Mahoney et al. 2006). This protocol can be conducted by preparing agar plates coated with *E. coli* and the assay of choice, where each agar plate is a different, uniform genotype of *C. elegans*. Keep in mind that the readout is only used as a proxy, and is not a direct measurement of ACh accumulation in the synaptic cleft. In addition, there may be minor variation in rates of paralysis between individuals, which can be affected by variables such as: individual variability, temperature, humidity, age of the aldicarb plates, and how the experimenter defines paralysis. This experiment is not practical when measuring large populations during the course of a single assay because it is impractical for the experimenter to score all nematodes individually given the time restriction (Mahoney et al. 2006). However, this point would hold for each of the protocols previously discussed since they too require agar plates as living conditions for nematodes.

An Aldicarb Experiment

In this study, I tested the hypothesis that vesicle acidification achieved by the V-ATPase proton pump, is a requirement for vesicle fusion to the terminal plasma membrane. Our knowledge of quantal size is limited, and we have yet to understand the properties that regulate it and the underlying mechanisms.

To test the effects of pH on quantal release, we measured the rate of nematode paralysis over time for different controls and mutant strains when treated with aldicarb (i.e. time course of aldicarb paralysis assay), which served as a proxy for the molecular action of the drug. We expected nematodes with gain-of-function mutations to have a higher rate of paralysis, whereas nematodes with partial loss-of-function mutations to have a lower rate of paralysis. We expected nematodes with gain-of-function mutations to experience an increase in V-ATPase activity, resulting in either an increased rate of neurotransmitter loading/vesicle fusion or increased quantal size (these mechanisms require further investigation). Despite which property underlies V-ATPase activity, we expected a faster accumulation of ACh in the synaptic cleft, leading to a higher rate of paralysis for these mutants. On the contrary, we expected partial loss-of-function mutations (resulting in decreased V-ATPase activity) to cause a decreased rate of neurotransmitter loading/vesicle fusion or decreased quantal size (which again, still require further investigation). As a result, we expected a slower accumulation of ACh in the synaptic cleft, leading to a slower rate of paralysis for these mutants. We expected wild-type (WT)

nematodes to have a rate of paralysis that falls in between that of the gain-of-function and partial loss-of-function mutants.

We have taken a new approach to candidate gene analysis to test this hypothesis. In particular, we tested candidate alleles which have been mapped by whole genome sequencing (Thompson et al. 2013), to determine whether alleles in our gene of interest have an aldicarb phenotype. A conventional screen for new mutants begins by randomly mutagenizing wild-type individuals, followed by a search of phenotypes of interest, and then a genetic screen/molecular mapping of the mutation (mutagenesis → phenotype screening → mapping) (Hardy et al. 2010). The million mutation project (MMP) (a collaborative community project) flipped this process around so that the researcher can screen previously mapped mutations for phenotypes of interest. The MMP aimed to generate multiple mutations in every *C. elegans* gene, and to build a complex library of these mutations and strains to a target depth of 15x genome coverage (Thompson et al. 2013). This project produced ~2,007 mutagenized strains containing approximately 400 missense mutations each, using EMS, ENU, or a cocktail of both (Thompson et al. 2013). The authors estimate a rate of 1% false positives and 7% false negatives for single nucleotide variants (SNVs) across all mutations. The source for our mutations in the V-ATPase gene, *vha-12*, were whole-genome sequenced "VC" strains, which were mutagenized using an EMS plus ENU cocktail from the MMP (VC is a lab designation of the primary laboratory where the project was headquartered, the C. elegans Reverse Genetics Core Facility, Vancouver, B.C., Canada, Donald Moreman).

We used a wild-type strain (N2) and a known resistant mutant strain (MT7907), as controls. MT7907 nematodes possess a mutation at position 4192683 in the *vha-12* gene on the X-chromosome, which encodes for the B subunit of the V_1 sector of the V-ATPase proton pump

(Ernstrom et al. 2012). A PCR experiment and DNA purification were performed prior to the assay to verify that all control and test strains possessed the correct genotype. The test subjects were various VC strains of unknown phenotypes, which all possess a point-mutation encoding for different components of the V_1 sector of the V-ATPase proton pump. We tested the following VC strains of interest: VC40421, VC40512, VC40082, and VC40914. The VC40421 strain contains a *vha-12(gk629998)X* missense mutation, where adenine was replaced with cytosine at nucleotide number 4192492, leading to an I249L amino acid change (Thompson et al. 2013). The VC40512 strain contains a *vha-12(gk672728)X* missense mutation, where guanine was replaced with adenine at nucleotide number 4192492, leading to an E433K amino acid change (Thompson et al. 2013). The VC40082 strain contains a *vha-12(gk277575)X* missense mutation, where cytosine was replaced with thymine at nucleotide number 4192382, leading to an S396F amino acid change (Thompson et al. 2013). Finally, the VC40914 strain contains a *vha-12(gk879986)X* missense mutation, where guanine was replaced with adenine at nucleotide number 4192683, leading to an E481K amino acid change (Thompson et al. 2013).

I define a single experiment as follows. An experiment is one assay for ~20 young adult worms for each of the following strains: the wild-type control strain (N2), the partial loss-of-function control (MT7907), and one "VC" strain of unknown phenotype. To further minimize bias during the experiment, the individual scoring the assay was blinded to the genotypes of the three strains prior to each assay. We will be comparing the survival proportions across strains at each time point during the assay in order to determine the associated aldicarb sensitivity phenotype of each VC strain of interest. By determining the aldicarb sensitivity phenotype for each VC strain, we can make deductions regarding the molecular effects of their respective genetic mutations in the V-ATPase and quantal release.

If the data were to support the fusogen model, we would expect no difference between the survival proportions of one or more of the VC strains and the N2 strain with aldicarb treatment. However, if the data were to support our hypothesis outlined by the pH model, we would expect a significant difference between the rate of paralysis between the one or more of the VC strains and the N2 strain with aldicarb treatment. Comparison between the rate of paralysis of VC strains and the rate of paralysis of the MT7907 will determine if the mutation in the test strain is a partial loss-of-function mutation. Comparison between the wild-type strain and the VC strains will determine whether the mutation is a gain-of-function mutation or if it has no significant effect on the phenotype. In particular, the discovery of a gain-of-function VC mutant with a *vha-12* mutation operating in the V_1 sector of the V-ATPase proton pump would strongly refute the hypothesis proposed by the fusogen model, which proposes mechanisms involving the V_o sector as the regulator of quantal release.

Methods

Chemicals and Enzymes

Chemicals for solutions and media were ACS grade unless otherwise stated. Millipore-Sigma (St. Louis, MO) was the source for salts, agar, cholesterol, and bacto-peptone for Nematode Growth Medium (NGM) (Brenner, 1974). PCR reagents were obtained from New England BioLabs (Ipswich, MA). Proteinase K was obtained from Thermo-Fisher Scientific.

Strains

C. elegans strains were obtained from the Caenorhabditis Genetics Center (funded by the National Institutes of Health - Office of Research Infrastructure Programs (P40 OD010440), and received in October 2023), with the exception of the N2 and MT7907 which were received from the Jorgensen Laboratory in Salt Lake City, Utah.

Our study focused on variants of the *C. elegans* gene, *vha-12,* which encodes the *C. elegans* ortholog of the B subunit of the V_1 sector of the V-ATPase proton pump (Ernstrom et al. 2012). The wild-type X-linked *vha-12* gene encodes a 491 amino acid protein, VHA-12. The following table lists the strain names, the *vha-12* genotype, and the nature of the missense mutation in the *vha-12* mutants analyzed in this study.

Strain Name	*vha-12 Genotype*	Mutation Type	Nucleotide Substitution	Codon Mutation
N2	*vha-12(+) X*	None	None	wild-type
MT7907	*vha-12(n2915sd) X*	transition	C 4192349 T	Ala 385 Valine
VC40421	*vha-12(gk629998)) X*	transversion	A 4191940 C	Ile 249 Leu
VC40082	*vha-12(gk277575) X*	transition	C 4192382 T	Ser 369 Phe
VC40512	*vha-12(gk672728) X*	transition	G 4192492 A	Glu 433 Lys
VC40914	*vha-12(gk879986) X*	transition	G 4192683 A	Glu 481 Lys

The MT7907 phenotypes are as follows: locomotion variant (Unc) with an abnormal "loopy" or "kinked" resting posture on solid agar medium; aldicarb resistant (Ric), slow growth (Gro), reduced brood size; variable molt defect (Mlt); and heterozygous-specific body-length variant (Dpy) (Ernstrom et al. 2012). Alternatively, VC40421 contains 436 mutations including a nucleotide substitution in the coding sequence of *vha-12* at nucleotide position 4191940 A → C on chromosome X (Thompson et al. 2013). VC40082 contains 243 mutations including a nucleotide substitution in the coding sequence of *vha-12* at nucleotide position 4192382 C → T on chromosome X (Thompson et al. 2013). VC40512 contains 315 mutations including a nucleotide substitution in the coding sequence of *vha-12* at nucleotide position 4192492 G → A on chromosome X (Thompson et al. 2013). Lastly, VC40914 contains 414 mutations including a nucleotide substitution in the coding sequence of *vha-12* at nucleotide position 4192683 G → A on chromosome X (Thompson et al. 2013).

C. elegans Cultivation

C. elegans nematodes were grown using standard procedures as described by Brenner (1974) and Stiernagle (2006). Specific materials, equipment, and quinities used in our preparations are as follows.

Food for *E. coli* was the liquid growth medium, Lauria-Bertani (LB) broth. A 2.5% (w/v) solution of 500ml LB broth was prepared combining granulated LB medium and ultrapure water. The mixture was stirred over light heat until fully dissolved, and subsequently divided into five, 100ml aliquots. The aliquots were autoclaved at 120˚C for 15 minutes in a Steris autoclave (Amsco Lab 250), and then stored at room temperature.

Nematode growth medium (NGM) is the agar-based substrate on which *C. elegans* are grown (Stiernagle, 2006). NGM consists of agar, bacto-peptone, and sodium chloride supplemented with salts and cholesterol as described by Stiernagle (2006) and Brenner (1974). One molar potassium phosphate buffer, a component of NGM, was prepared by combining 108.3 g of KH_2PO_4 (potassium phosphate monobasic) and 35.4 g of K_2HP04_2 (potassium phosphate dibasic) with ultrapure water, which was stirred over light heat until fully dissolved. A pH meter was used to measure the pH of the mixture. KOH was added to the solution until a pH of exactly 6 was reached. The volume of the solution was finalized to the desired amount with ultrapure water. The $KHPO_4$ buffer solution was subsequently divided into 10, 100ml aliquots, which were autoclaved at 120˚C for 15 minutes, and then stored at room temperature for later use. A similar process was repeated using solid $MgSO_4$ and solid $CaCl_2•2H_2O$ for the preparation of 500ml 1M $CaCl_2•2H_2O$ and 500ml 1M $MgSO_4$ solutions.

The NGM solution was prepared by combining 3g NaCl, 17g agar, and 2.5 g bacto-peptone (product #211677) into a 2L erlenmeyer flask with 975ml of ultra-purified

deionized water. The solution was stirred over light heat until fully combined, and then autoclaved for 30 minutes at 121˚C. Nematode growth medium requires salt and cholesterol supplements that are added to molten NGM after it has cooled to about 55°C, which prevents salt precipitation. 1ml of 1M $CaCl_2$•$2H_2O$, 1ml 5mg/ml cholesterol in ethanol, 1ml of 1M $MgSO_4$, and 25ml of 1M $KHPO_4$ buffer were added to the sterile flask (in that order). Using sterile conditions, ~11-12ml of 55˚C NGM solution was added into 60mm petri dishes using a peristaltic pump (Wheaton Unispense). The NGM plates were left undisturbed at room temperature for 2-3 days to allow for contaminants to be detected and moisture to evaporate. Uncontaminated plates were stored in plastic containers at 4˚C to be used for several weeks.

E.coli OP50 (grown at 37 with 200 rpm shaking) was used as a food source for *C.elegans* development. Using sterile conditions, NGM plates were streaked with OP50 (obtained from the Jorgensen Lab, Salt Lake city, Utah) in order to begin a starter culture. The streaked plates were stored at 4˚C. A 100ml aliquot of liquid LB broth was antiseptically inoculated using a single colony collected from one of the streaked NGM plates. The remaining NGM plates were sterilely seeded with OP50 by pipetting 1-2 droplets (10-20µl) of the uncontaminated, inoculated liquid LB broth onto the center of fresh NGM plates. To create a bacterial lawn, a sterilized bent glass pipet tip was used to spread the inoculated LB broth droplets. Inoculated NGM plates were allowed to sit for one to two days at room temperature to form a bacterial lawn. Additional inoculated NGM plates were subsequently stored at 4˚C to be used later during *C.elegans* cultivation.

C. elegans strains were cultured by chunking or picking ~10-20 worms of each strain to a new seeded NGM plate. Cultured NGM plates were delineated with the date, the strain name, and the genotype written around the perimeter of the plate. This process was completed for each

C. elegans strain in rotation approximately 3 times per week. *C. elegans* strains that were not in rotation were picked or chunked approximately once per month and stored in an incubator at 20˚C to slow development of the population. Additionally, some plates for each strain were starved and stored at -20˚C for preservation and future use.

Nematode Husbandry

Strains used in this study were cultivated as originally described by Brenner (1974), and detailed by Stiernagle (2006). Briefly, strains were maintained by passaging adult hermaphrodites to fresh NGM agar petri plates (60 mm) inoculated with OP50 *E. coli* bacteria as the nematode food source. OP50 is a slow-growing uracil auxotroph, and when approximately 10μL is spread across the surface of the agar medium, a thin lawn is formed overnight at room temperature (20-22°C). Such a lawn provides food, but is not too thick as to obscure the movement or visualization of animals. These bacterial seeded plates were stored at 4℃ and brought to room temperature prior to passaging. Stocks were maintained at room temperature or in an incubator set to 20°C. To passage a particular strain from a plate to a fresh plate with food, at least ten hermaphrodite individuals were transferred with a heat-sterilized platinum wire called a "worm-pick." Subpopulations were also cloned using a standard, heat-sterilized chemical spatula to excise a square centimeter chunk of agar from an overgrown plate, and placing that chunk on a fresh OP50 seeded NGM plate.

Single-Worm PCR

The procedure for single-worm PCR was modified from Williams et al. 1992. A single worm lysis buffer (SWLB) of 50mM KCl, 10mM Tris•HCl (pH 8.3) 2.5mM $MgCl_2$, 0.45%

IGEPAL, 0.45% Tween20, and 1mg 0.01% gelatin were combined into a falcon tube. Ultra-purified deionized water was added until the solution measured to 10ml total. The mixture was divided into 10, 1ml aliquots. Proteinase K (Sigma-Aldrich) was diluted to 1mg/ml with the lysis buffer prior to SWLB use. All solutions containing active enzymes were kept on ice while actively being used. The SWLB was stored at -20˚C for later use.

Three-to-five worms of uniform genotype were handpicked and placed into the cap of a PCR tube with 10µl of SWLB (containing proteinase K), and the solutions were centrifuged. This process was repeated for each *C. elegans* strain. A negative control was prepared such that it contained only 10µl of SWLB, and no worms. The PCR tubes were frozen at -80˚C for at least 10 minutes. Once removed from the freezer, the solution was thawed on ice (for a couple of minutes), and placed in a thermal cycler (Bio-rad, T100) to be incubated at 65˚C for 1 hour, and subsequently heat inactivated at 95˚C for 15 minutes.

A PCR master mix enough for one reaction (modified from and supplied by the New England BioLabs *Taq* PCR Kit protocol) was made by combining 10µl 10x standard *Taq* reaction buffer, 2µl 10mM deoxynucleotides (dNTPs), 2µl 10µM oGE12 forward primer (5'-CGT ATC TAT CAA TGT ATC TGC CAC-3') (IDT Integrated DNA Technologies), 2µl 10µM oGE22 reverse primer (5'-GTT GGA TTT CCA GCT ATC AC-3') (IDT Integrated DNA Technologies), 0.5µl *Taq* DNA Polymerase, and 63.5µl nuclease-free water into a microfuge tube. The volumes of the master mix components were multiplied by the number of PCR reactions run (if more than one was run). Approximately 80µl of this master mix solution was added to the 10µl of Lysis solution (template DNA) for each strain and the negative control. The temperature settings for the Biorad T100 Thermal Cycler were modified per the New England BioLab *Taq* PCR protocol. The PCR solutions underwent an initial denaturation at 95˚C for 30 seconds, followed by 30

cycles of the following: 30 seconds at 95˚C, 30 seconds at 60˚C, and 2 minutes and 30 seconds at 68˚C. A final extension was run at 68˚C for 5 minutes, and the products were held at 4˚C.

Electrophoresis gel was prepared by combining 50ml 1x TAE with 0.6g solid agarose in a 250ml glass flask. The flask was covered and heated in a microwave for ~40 seconds. The solution was allowed to cool for ~10 minutes. After it had cooled enough to be handled, 5µl of 10,000x GelRed Nucleic Acid (Biotum) was added into the 250ml flask containing the agarose solution. Prior to pouring, the gel electrophoresis device was assembled by inserting the thin, 10-welled comb into the casting tray. The agarose solution was poured about ½ the way up the casting tray, and was allowed to rest for ~30 minutes until the gel had set.

Prior to loading the samples, enough 1x TAE was poured over the top of the agarose gel to completely submerge it. 5µl of each of the PCR products were combined with 1µl of 6X NEB Gel Loading Dye, separately. 6µl of the 1kb ladder was loaded into the first well, followed by 6µl of the PCR products in each of the following wells. The gel was run at 100V (60 mA) for 45 minutes. The product was visualized under a UV light.

DNA Purification

DNA for each *C.elegans* strain was purified and quantified to ensure the quality and presence of desired DNA in each mutant assayed. The materials for DNA purification were the Zymo Research DNA Clean and Concentrator Kit, and DNA purification on all PCR samples was performed according to manufacturer protocol. Following DNA purification, the ultra-pure DNA for each strain was quantified and recorded using a NanoDrop 2000/2000c spectrophotometer (ThermoFisher Scientific) according to the manufacturer's protocol.

Aldicarb Assay

An aldicarb assay was performed in order to characterize the aldicarb sensitivity phenotypes associated with genetically characterized V-ATPase mutants. The preparation and assembly of aldicarb plates were adapted from Oh and Kim, 2017. A 100 mM aldicarb stock was made by dissolving 100 mg analytical-grade aldicarb (ChemService, West Chester, PA) in 5.25 mL 70% ethanol and stored at -20˚C. To make 1 mM aldicarb assay plates, 1 mL of 100 mM aldicarb stock solution was added to a final volume of 100 mL. Plates were stored at 4˚C prior to use.

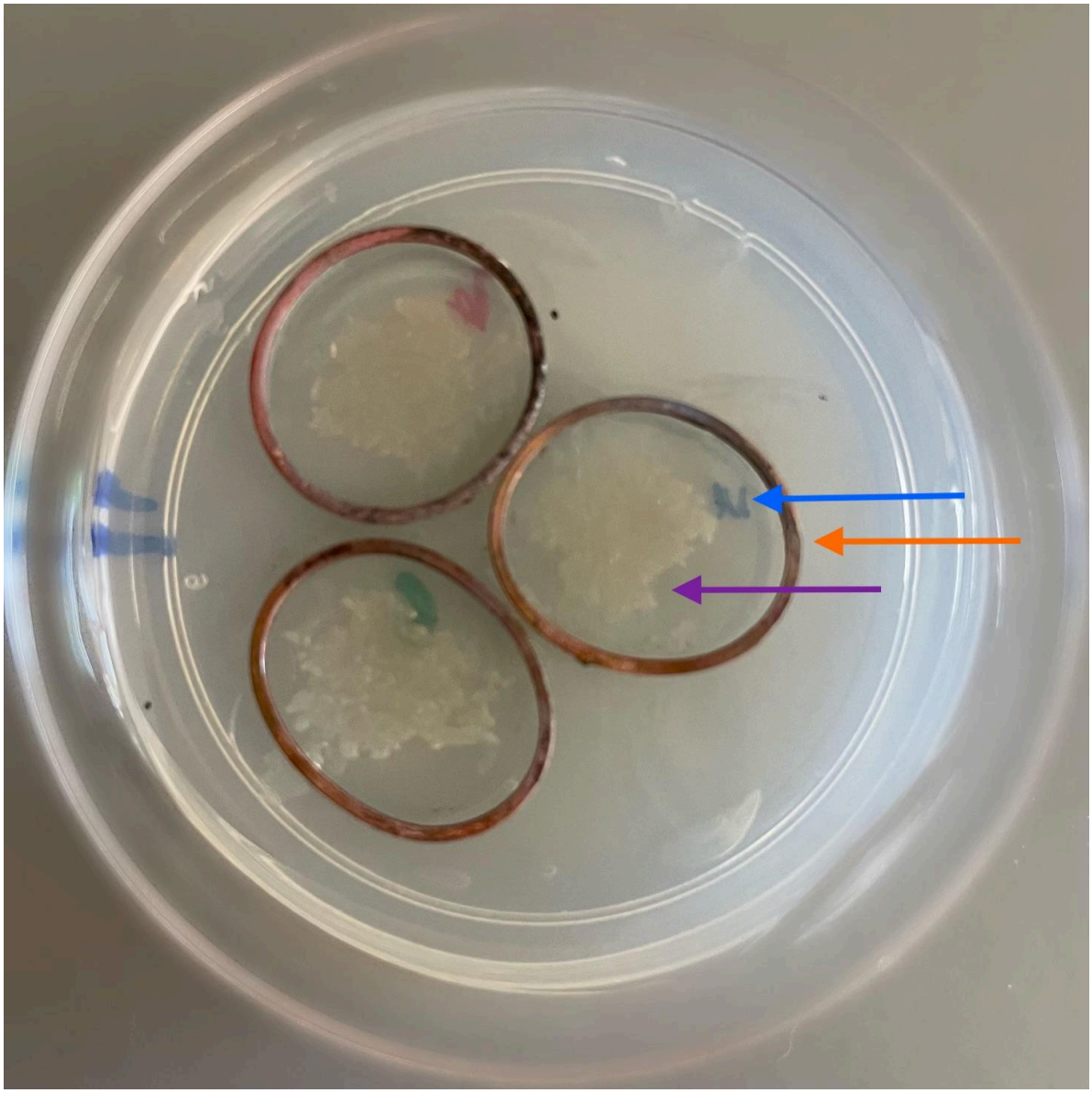

Figure 4. Aldicarb plate assembly. I was blinded to the genotype during the assay by a colleague who labeled the underside of the plate under each ring (orange arrow) with a marker spot (indicated by the blue arrow) of either blue, red, or green which corresponded to either the the wild-type control strain (N2), a known aldicarb resistant strain (MT7907), and a test VC strain. Colors and genotypes were randomized for each assay, and the color codes were recorded by the individual scoring the assay in a spreadsheet. The OP50 food source (purple arrow) was spotted in the middle of each copper ring.

In order to stage worms for the assay, between 30-40 L4 worms for each control/test strain (N2, MT7907, and a VC strain of choice) were isolated onto separate, OP50 seeded NGM plates on the night before each assay. The following day, three sterile copper rings were added to an aldicarb plate equally spaced apart, which served as corrals to segregate strains during the assay (**Figure 4**). The center of each ring was spotted with OP50 (**Figure 4**). Using a sterile worm pick loaded with OP50, a colleague uniformly picked and placed approximately 20 individuals for each strain into the center of their respective copper rings. Strain placement was staggered by 3-4 minutes to allow time for measurements, and the times at which each strain was loaded onto the aldicarb plate were recorded. The strains were denoted with colors (such as blue, green, and red) to the blinded individual scoring the assay.

An initial count of the number of living individuals for each strain were recorded on a spreadsheet at time point "zero," during their placement onto the aldicarb plate. Measurements for each strain were taken at ten minute intervals from the time they were loaded onto the aldicarb plate. These measurements included the total number of individuals observed at each timepoint, the total number of individuals paralyzed at each time point, the total number of individuals missing at each time point, the total number of living individuals at each time point, and additional observations (for each strain). Missing individuals were not included in the total for the number of individuals observed, however both paralyzed and live individuals were.

Individuals were qualified as missing if they escaped their copper ring, had burrowed into the aldicarb NGM media, had died from a cause other than paralysis, or could not be found. Paralysis was qualified as complete cessation of movement in response to 3 consecutive gentle pokes or strokes with a worm pick. The measurements were compiled in a spreadsheet document and saved for later analysis during data processing. The assay was generally run until the last

individual across all three strains had paralyzed, or sometimes until a few individuals remained and significant time had passed since documentation of the most recent death. All worms were visualized under a dissecting microscope in order to plate the correct number of worms and properly score each paralysis event.

Data Analysis

Data were input into GraphPad Prism 10.2.0 to run survival analyses and generate graphs. To account for censored data (i.e. individuals that escaped from the scoring arena, effectively "dropping out of the study") a Kaplan-Meier survival curve was generated in order to estimate the probability of survival for each strain over the time course of an assay. For all analyses, both individual data (from a single assay) and compiled data (data across all three trials for a VC strain of interest merged into one superset) were processed. A trial is defined here as an independent experiment performed on a single day that includes the concurrent survival measurements of wild-type, *vha-12(n2915)*, and a particular "VC" strain. A Mantel-Cox test was conducted in order to compare the survival distributions across strains, over time. Since three groups were compared simultaneously, an adjusted threshold for significance was determined using a Bonferroni-corrected α value. This was computed using the equation $\alpha_{Bonferroni} = \frac{\alpha_{family}}{K}$, where K is the number of comparisons made, and α_{family} is the α threshold for significance that one wishes to apply to an entire family of comparisons (for all multiple comparisons, this was 0.05). The Bonferroni-corrected α value for all analyses was 0.01667. Additionally, a post hoc multiple comparisons test was run in order to make pairwise comparisons between individual strains. A threshold for significance of $p < 0.05$ was used.

Results

The goal of this thesis was to identify *vha-12 C.elegans* mutant strains that would be valuable in defining the role of the V-ATPase proton pump in neurotransmitter release. *C. elegans* were scored for an aldicarb paralysis phenotype by conducting a genotypically-blinded time course to aldicarb paralysis assay using twenty young adult worms of uniform genotype (resistant MT7907 control, wild-type N2 control, and a VC test-strain), which were plated into the center of distinct copper rings on a 1mM aldicarb plate. We predicted that partial loss-of-function mutations in the V_1 sector of the V-ATPase would result in resistant aldicarb paralysis phenotypes. Alternatively, we predicted that gain-of-function mutations in the V_1 sector of the V-ATPase would lead to hypersensitive aldicarb paralysis phenotypes. We hypothesized that hypersensitive phenotypes would be a result of accelerated vesicle acidification, leading to enhanced vesicle fusion and neurotransmitter release. Instead, resistant phenotypes would be induced by reduced vesicle acidification, resulting in diminished vesicle fusion and neurotransmitter release.

The four VC strains tested in this study were VC40421 (expressing a *vha-12(gk629998)X* missense mutation and an I249L amino acid change 130 and 102 positions away from the arginine and tyrosine catalytic sites, respectively), VC40512 (expressing a *vha-12(gk672728)X* missense mutation and an E433K amino acid change 54 and 82 positions away from the arginine and tyrosine catalytic sites, respectively), VC40082 (expressing a *vha-12(gk277575)X* missense mutation and an S396F amino acid change 17 and 45 amino acids away from the arginine and tyrosine catalytic sites, respectively), and VC40914 (expressing a *vha-12(gk879986)X* missense mutation and an E481K amino acid change 102 and 130 positions away from the arginine and tyrosine catalytic sites, respectively) (Ernstrom et al. 2012; Thompson et al. 2013). Below we

have outlined the results for the survival probabilities and corresponding aldicarb paralysis phenotypes of each of these mutant strains compared to known resistant and wild-type controls. We define an experiment as one assay consisting of ~20 young adult worms for the N2 strain, the MT7907 strain, and one "VC" strain of unknown phenotype. All statistical tables can be found in Appendix A.

All nematodes, regardless of genotype, exhibited paralysis in response to the aldicarb nematicide. The survival probability did not differ from wild-type for the first, second, and third VC40512 assays (**Figure 5 (a, b, c) , Table A1, Table A2**: two-way Mantel-Cox, Experiment 1: $p = .0589$, Experiment 2: $p = .8499$ Experiment 3: $p = .614$). These data were consistent with the collapsed data set for all three VC40512 assays (**Figure 6, Table A1, Table A2**: two-way Mantel-Cox, $p = .565$).

A three-way Mantel-Cox test also indicated a significant difference in the survival probability across strains for the first and second VC40082 assays (**Figure 7 (a, b), Table A1**: three-way Mantel-Cox, Experiment 1: $p = .0107$, Experiment 2: $p = .0001$), but not for the third (**Figure 7 (c), Table A1**: three way Mantel-Cox, $p = .0239$). A two-way Mantel-Cox test was run in order to determine differences in survival probability between strains for the VC40082 assays. The survival probability of VC40082 was significantly different than that of N2 across all three trials, however these differences were not consistent. The first and second trials indicate that the probability of survival for VC40082 was significantly lower across time intervals compared to N2 (**Figure 7 (a, b), Table A3**: two-way Mantel-Cox, Experiment 1: $p = .0005$, Experiment 3: $p = .0003$), whereas the third trial indicates that the probability of survival for VC40082 was significantly higher compared to N2 (**Figure 7 (c), Table A3**: two-way Mantel-Cox, $p = .0136$). Additionally, a two-way Mantel-cox indicated that the probability of

survival for VC40082 was significantly higher than MT7907 for the third assay (**Figure 7 (c), Table A3:** two-way Mantel-Cox, p = .0438), and significantly lower than MT7907 for the second assay (**Figure 7 (b), Table A3:** two-way Mantel-Cox, p = .001). However, no significant difference was indicated for the first assay. Statistical analysis of the collapsed data set for VC40082 assays indicated no significant difference in the survival probability across strains (**Figure 8, Table A1, Table A3**: three-way Mantel-Cox, p = .3108).

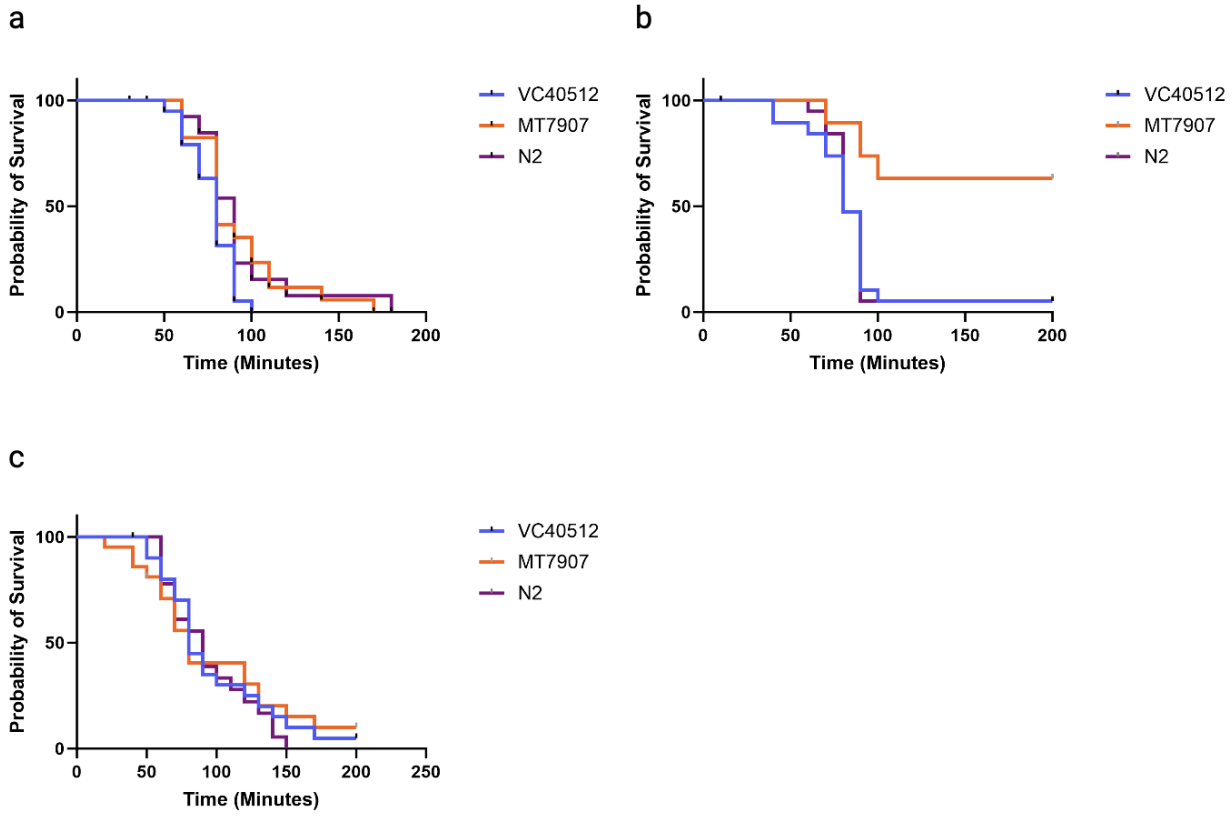

Figure 5. The V_1 sector V-ATPase *C. elegans* mutant, VC40512, exhibits a nonsignificant aldicarb paralysis phenotype. Kaplan-Meier survival curves depicting the probability of survival over the course of ten-minute time increments of 20 staged resistant control MT7907 (orange), wild-type control N2 (purple), and VC40512 test-strain (blue) *C. elegans* nematodes, for the first (**a**), second (**b**), and third (**c**) VC40512 test-strain aldicarb assays. For all assays, paralysis was qualified as the lack of physical movement following three, consecutive gentle pokes with a worm pick, which was visualized under a dissecting microscope.

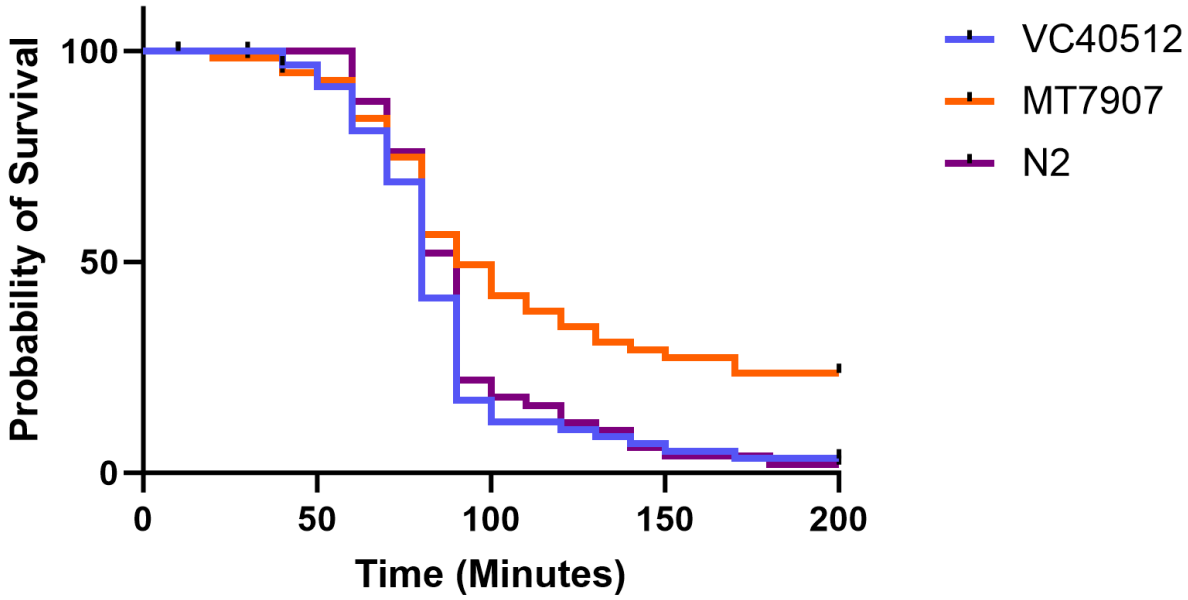

Figure 6. Collapsed data for the V_1 sector V-ATPase *C. elegans* mutant, VC40512, indicates a nonsignificant aldicarb paralysis phenotype. The graph above depicts a Kaplan-Meier survival curve for collapsed data across all three VC40512 experiments. A collapsed data set is a combined data set, where data for all three VC40512 experiments were joined into one large data set. These graphs depict the probability of survival over the course of ten-minute time increments for ~50-60 staged resistant control MT7907 (orange), wild-type control N2 (purple), and VC40512 test-strain (blue) *C. elegans* nematodes, respectively. For all assays, paralysis was qualified as the lack of physical movement following three, consecutive gentle pokes with a worm pick, which was visualized under a dissecting microscope.

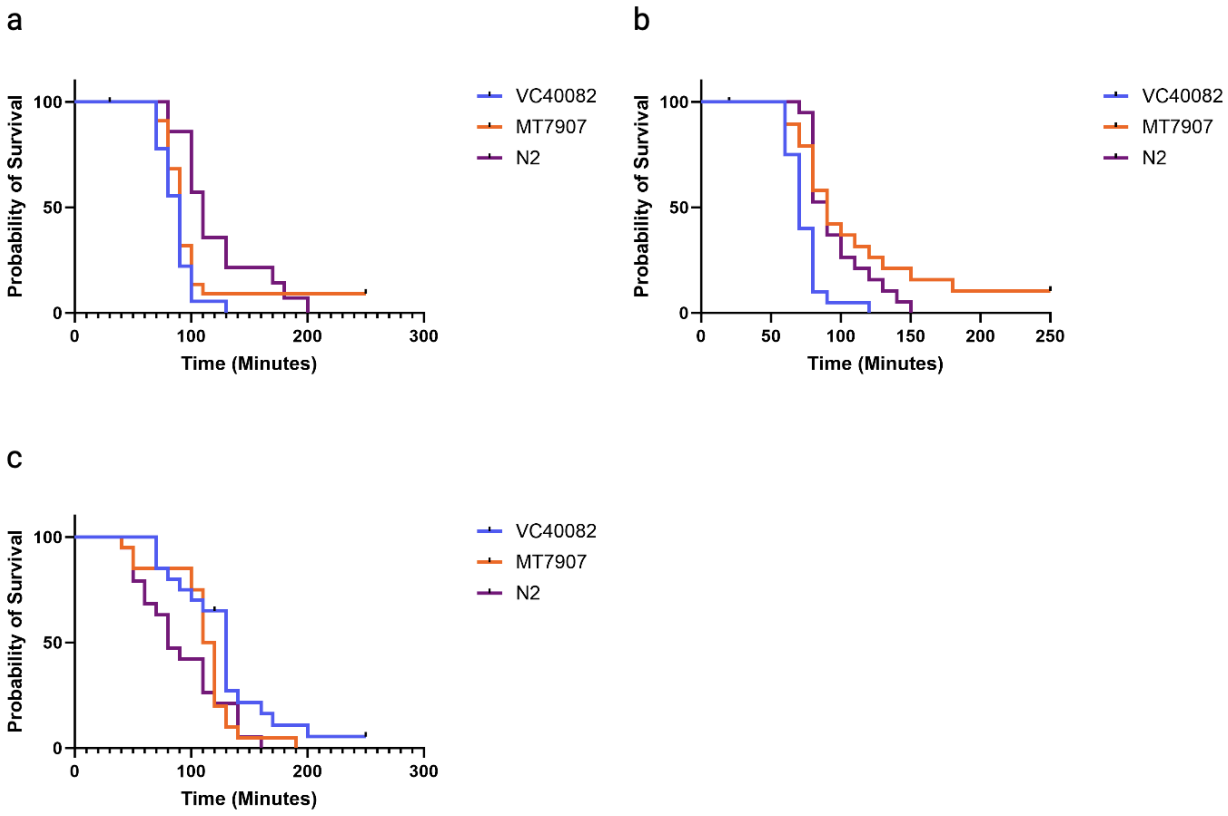

Figure 7. The V_1 sector V-ATPase C. elegans mutant, VC40082, exhibits an overall nonsignificant aldicarb paralysis phenotype. Kaplan-Meier survival curves depicting the probability of survival over the course of ten-minute time increments of 20 staged resistant control MT7907 (orange), wild-type control N2 (purple), and VC40512 test-strain (blue) *C. elegans* nematodes, for the first (**a**), second (**b**), and third (**c**) VC40082 test-strain aldicarb assays. For all assays, paralysis was qualified as the lack of physical movement following three, consecutive gentle pokes with a worm pick, which was visualized under a dissecting microscope.

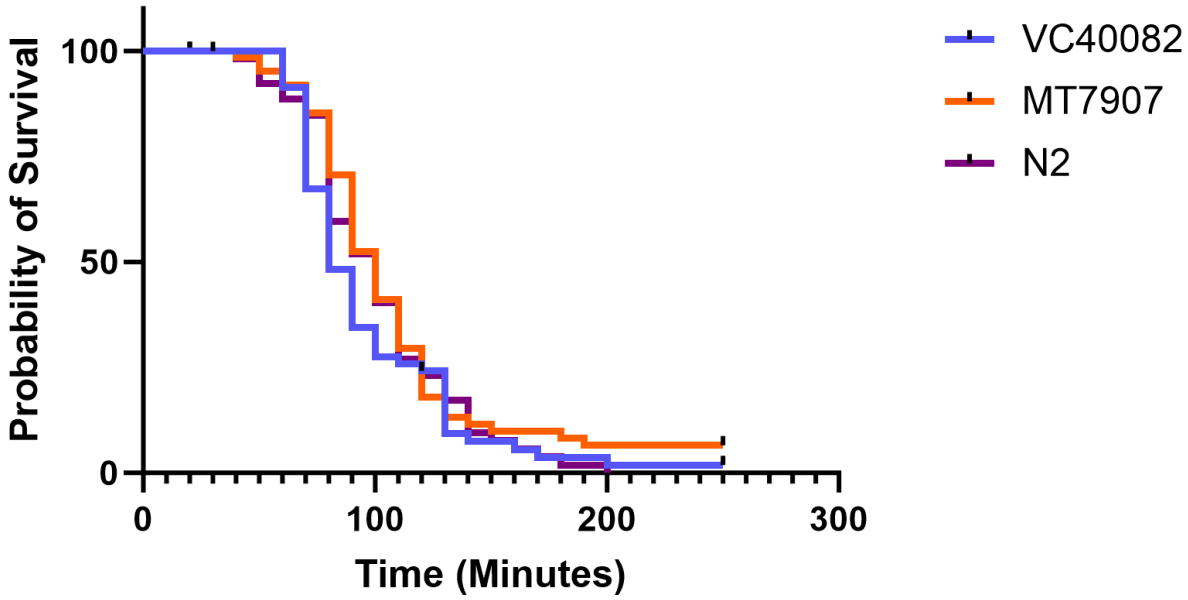

Figure 8. Collapsed data for the V_1 sector V-ATPase *C. elegans* mutant, VC40082, indicates a nonsignificant aldicarb paralysis phenotype. The graph represented above depicts a Kaplan-Meier survival curve for collapsed data across all three VC40082 experiments. A collapsed data set is a combined data set, where data for all three VC40082 experiments were joined into one large data set. These graphs depict the probability of survival over the course of ten-minute time increments for ~50-60 staged resistant control MT7907 (orange), wild-type control N2 (purple), and VC40512 test-strain (blue) *C. elegans* nematodes, respectively. For all assays, paralysis was qualified as the lack of physical movement following three, consecutive gentle pokes with a worm pick, which was visualized under a dissecting microscope.

A three way Mantel-Cox test also determined significant differences in the survival probabilities across control and test strains for the VC40421 assays (**Figure 9 (a, b, c), Table A1**: three-way Mantel-Cox, Experiment 1: $p < .0001$, Experiment 2: $p < .0001$, Experiment 3: $p < .0001$). The survival probability of VC40421 was significantly lower than both N2 (**Figure 7 (a, b, c), Table A4**: two-way Mantel-Cox, Experiment 1: $p < .0001$, Experiment 2: $p < .0001$, Experiment 3: $p < .0001$) and MT7907 (**Figure 9 (a, b, c), Table A4**: two-way Mantel-Cox,

Experiment 1: $p < .0001$, Experiment 2: $p < .0001$, Experiment 3: $p < .0001$) across all three trials, which is consistent with collapsed data set analysis for this strain (**Figure 10, Table A1, Table A4:** three-way Mantel-Cox, $p < .0001$)(**Figure 10, Table A4**: two-way Mantel-Cox, N2 vs. VC40421: $p < .0001$, MT7907 vs. VC40421: $p < .0001$,).

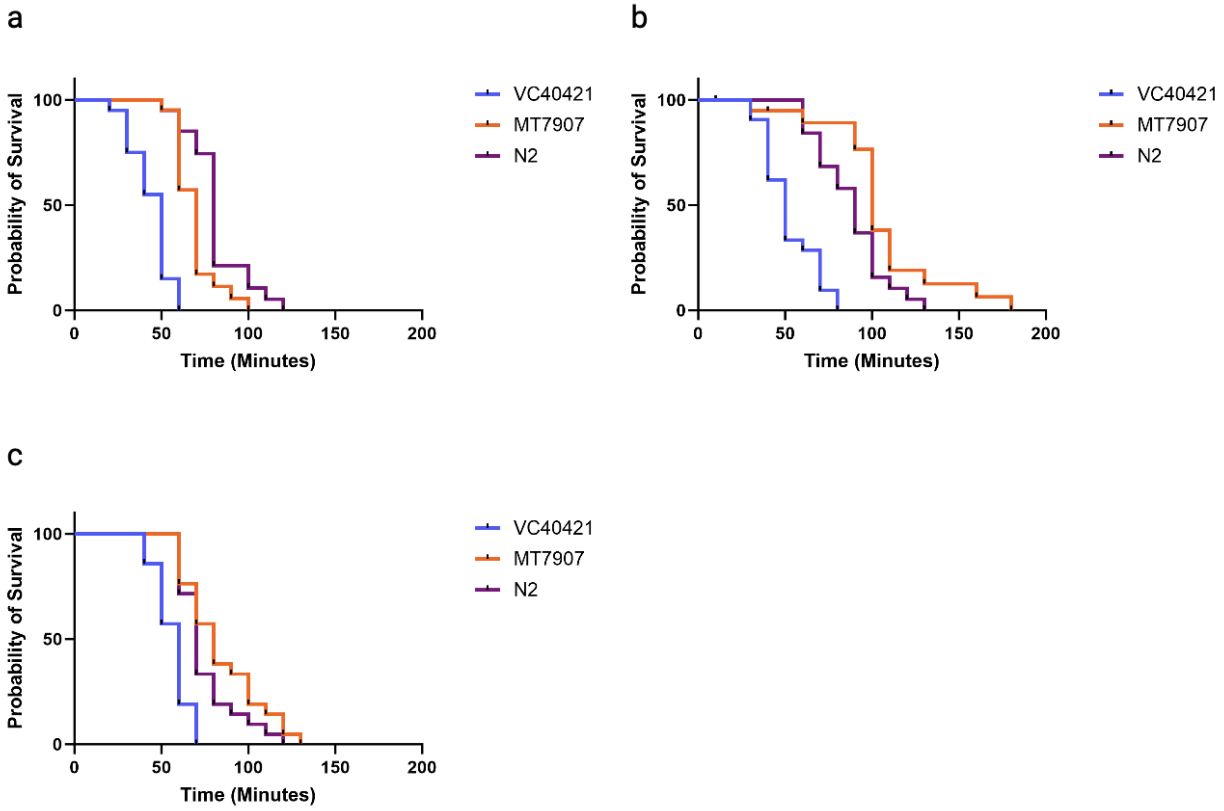

Figure 9. Gain of function V_1 sector V-ATPase *C. elegans* mutant, VC40421, exhibits a hypersensitive aldicarb paralysis phenotype. Kaplan-Meier survival curves depicting the probability of survival over the course of ten-minute time increments of 20 staged resistant control MT7907 (orange), wild-type control N2 (purple), and VC40512 test-strain (blue) *C. elegans* nematodes, for the first (**a**), second (**b**), and third (**c**) VC40421 test-strain aldicarb assays. For all assays, paralysis was qualified as the lack of physical movement following three consecutive gentle pokes with a worm pick, which was visualized under a dissecting microscope.

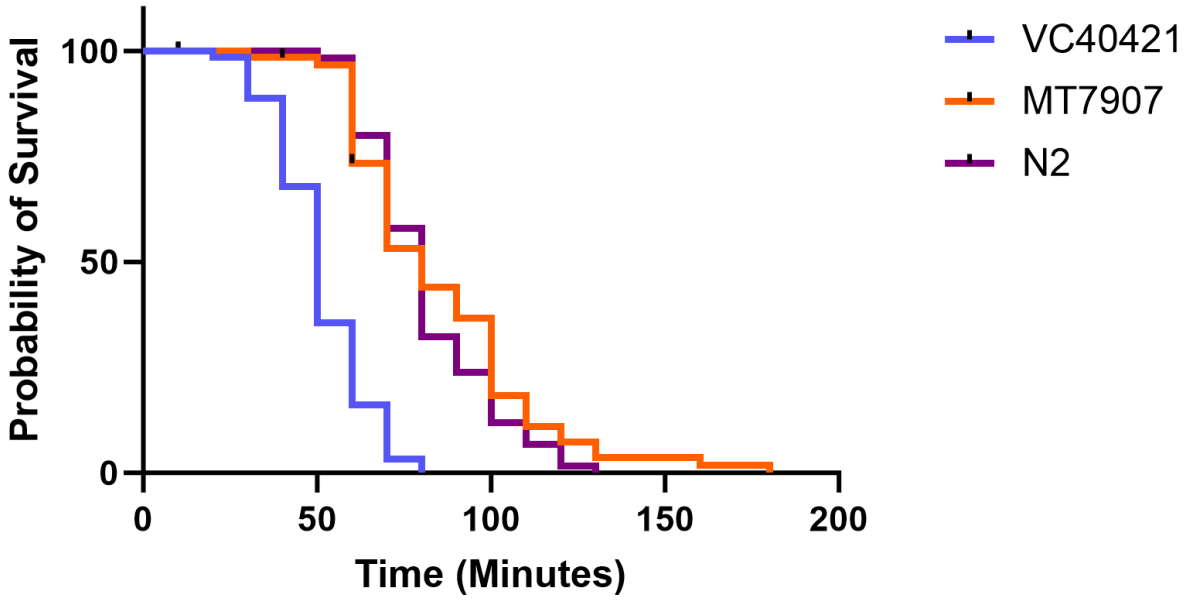

Figure 10. Collapsed data for the V_1 sector V-ATPase *C. elegans* mutant, VC40421, indicates a hypersensitive aldicarb paralysis phenotype. The graph represented above depicts a Kaplan-Meier survival curve for collapsed data across all three VC40421 experiments. A collapsed data set is a combined data set, where data for all three VC40421 experiments were joined into one large data set. These graphs depict the probability of survival over the course of ten-minute time increments for ~50-60 staged resistant control MT7907 (orange), wild-type control N2 (purple), and VC40512 test-strain (blue) *C. elegans* nematodes, respectively. For all assays, paralysis was qualified as the lack of physical movement following three, consecutive gentle pokes, which was visualized under a dissecting microscope.

Finally, a three-way Mantel-Cox test indicated significant differences in the survival probabilities across control and test strains for the VC40914 assays (**Figure 11 (a, b, c), Table A1**: three-way Mantel-Cox, Experiment 1: $p < .0001$, Experiment 2: $p < .0001$, Experiment 3: $p < .0001$). The survival probability of VC40914 was significantly higher than N2 for the second and third assays (**Figure 11 (b, c), Table A5**: two-way Mantel-Cox, Experiment 2: $p < .0001$, Experiment 3: $p < .0001$), but not the first (**Figure 11 (a), Table A5**: two-way Mantel-Cox, $p =$

.3505). Statistical analysis of the collapsed data set for VC40914 is consistent with the second and third assays (**Figure 12, Table A5**: two-way Mantel-Cox, $p < .0001$). There was no difference between the survival probability of VC40914 and MT7907 for the second and third trials (**Figure 11 (b, c), Table A5**: two-way Mantel-Cox, Experiment 2: $p = .2497$, Experiment 3: $p = .8027$), however, the probability of survival was significantly lower for VC40914 compared to MT7907, for the first trial (**Figure 11 (a), Table A5**: two-way Mantel-Cox, $p < .0001$). The collapsed data set for VC40914 was consistent with the MT7907 and VC40914 comparisons made for the first assay (**Figure 12, Table A5**: two-way Mantel-Cox, $p = .0065$). Additionally, the survival probability for MT7907 was significantly higher than that of N2 across all three trials (**Figure 12, Table A5**: two-way Mantel-Cox, $p < .0001$)(**Figure 11 (a, b, c), Table A5**: two-way Mantel-Cox, Experiment 1: $p < .0001$, Experiment 2: $p < .0001$, Experiment 3: $p < .0001$), which is consistent with prior characterization of the MT7907 phenotype. Earlier assays taken towards the beginning of data collection are not as consistent (**Figure 5 (a, c), Figure 7 (a, b, c), Figure 9 (a, c), Table A1, Table A2, Table A3, Table A4**). However, it was observed that the MT7907 resistant control strain tended to habituate and exhibit more subtle movements in response to prods with a worm pick, compared to VC40421 and N2. These discrepancies in scoring paralysis, particularly for MT7907, seemed to resolve through the course of data collection.

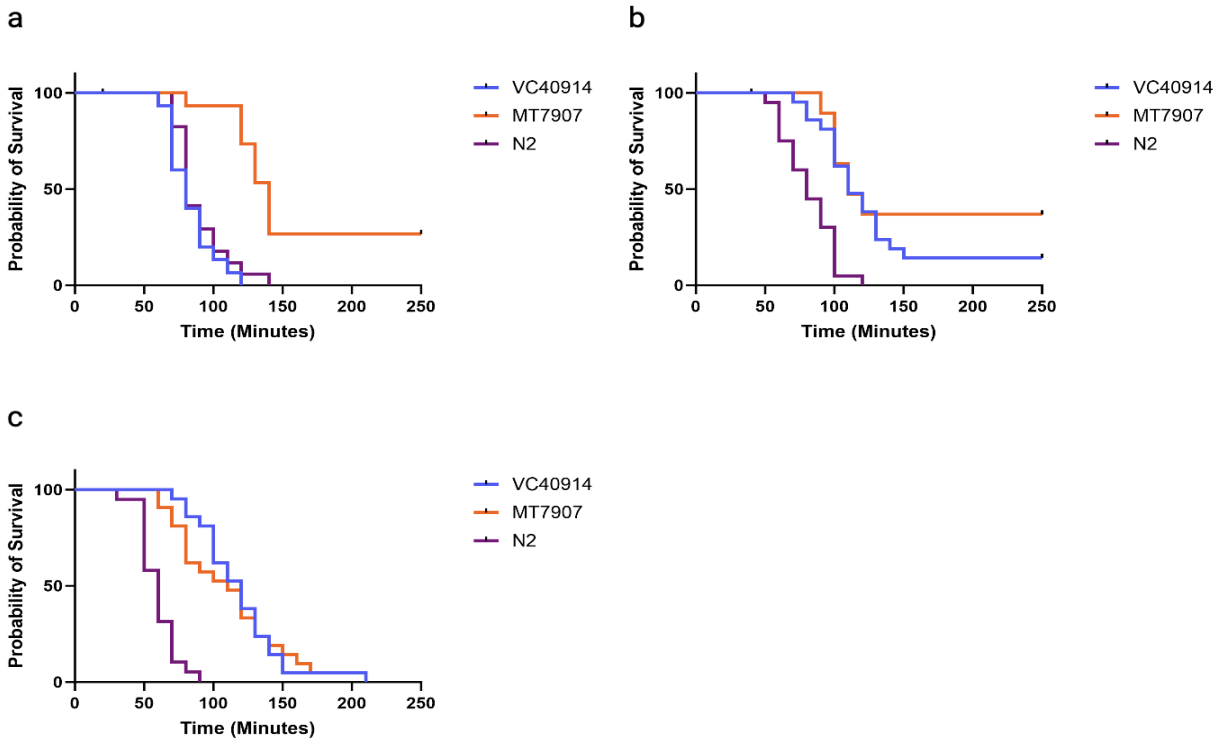

Figure 11. Loss of function V_1 sector V-ATPase *C. elegans* mutant, VC40914, exhibits a resistant aldicarb paralysis phenotype for most assays. Kaplan-Meier survival curves depicting the probability of survival over the course of ten-minute time increments of 20 staged resistant control MT7907 (orange), wild-type control N2 (purple), and VC40512 test-strain (blue) *C. elegans* nematodes, for the first (**a**), second (**b**), and third (**c**) VC40914 test-strain aldicarb assays. For all assays, paralysis was qualified as the lack of physical movement following three, consecutive gentle pokes with a worm pick, which was visualized under a dissecting microscope. It should be noted that for the first assay, there was a lack of L4 staged worms for all three strains (N2, MT7907, and VC40914), so only 15-18 worms were plated and assayed for each strain, rather than the typical 20.

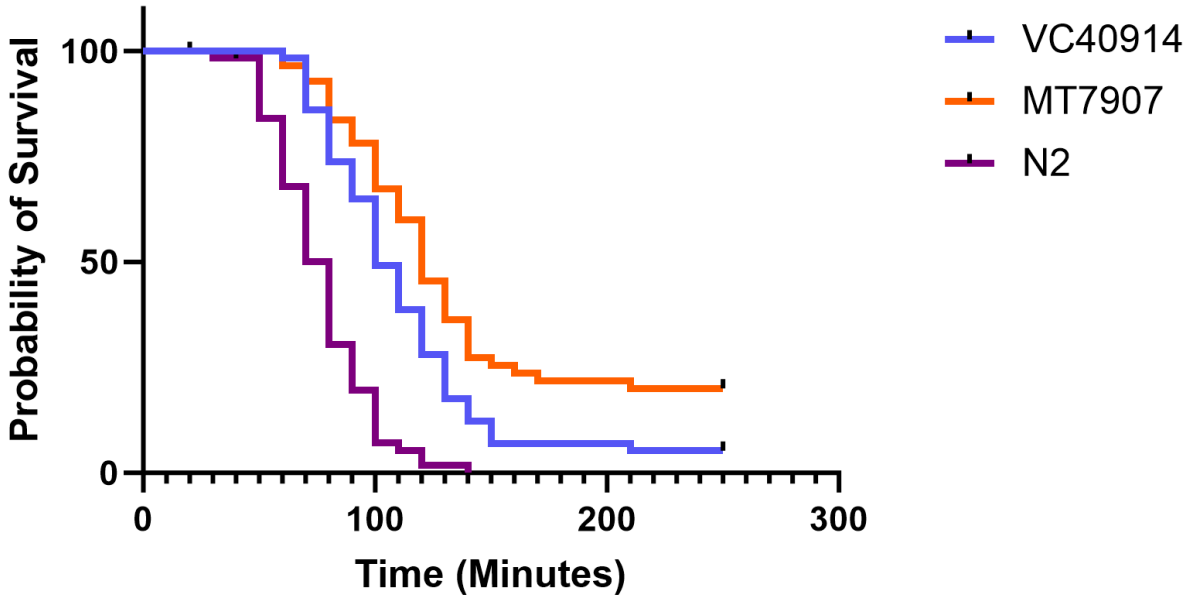

Figure 12. Collapsed data for the V_1 sector V-ATPase *C. elegans* mutant, VC40914, indicates a mildly resistant aldicarb paralysis phenotype. The graph represented above depicts a Kaplan-Meier survival curve for collapsed data across all three VC40914 experiments. A collapsed data set is a combined data set, where data for all three VC40914 experiments were joined into one large data set. These graphs depict the probability of survival over the course of ten-minute time increments for ~50-60 staged resistant control MT7907 (orange), wild-type control N2 (purple), and VC40512 test-strain (blue) *C. elegans* nematodes, respectively. For all assays, paralysis was qualified as the lack of physical movement following three, consecutive gentle pokes with a worm pick, which was visualized under a dissecting microscope.

Discussion

In this study, we addressed the question of whether the pH gradient achieved by the V-ATPase proton pump is a requirement for synaptic vesicle fusion. Whether synaptic vesicle acidification is a prerequisite for fusion is controversial and not established in the field of synaptic vesicle exocytosis. Evidence from prior work suggests that synaptic vesicle V-ATPases does promote fusion competency (Bodzeta et al. 2017), while other work is consistent with portions of the V-ATPase catalyzing a late step of synaptic vesicle fusion (Heisinger et al. 2005). More work is needed to resolve this question, but I believe that the discovery of synaptic phenotypes associated with two different *vha-12* alleles indicated by my results, provide a clear path forward to further testing a pH-checkpoint hypothesis.

We have sought to establish an allelic series of *vha-12* to investigate neurotransmitter release, which has been proven to be a valuable genetic approach in resolving biochemical pathways (Konopka and Benzer, 1971; Crouse et al. 2020). The *vha-12* gene encodes a subunit vital for the proton-pumping activity of the multisubunit V-ATPase complex. Only two *vha-12* alleles have been characterized with significant phenotypic changes: *vha-12(n2915sd)X*, a partial loss-of-function mutation used as a control in this study, and an embryonic lethal mutation, *vha-12(mg41)X* (Ernstrom et al. 2012). Our hypothesis predicts that a range of V-ATPase activity will correlate with changes in neurotransmitter release. For instance, gain-of-function variants would be expected to acidify vesicles faster than normal, accelerate the neurotransmitter loading process, and make a larger quantity of vesicles fusion competent. We would also predict these gain-of-function mutants to be hypersensitive to the acetylcholinesterase inhibitor, aldicarb. Aldicarb hypersensitivity is consistent with increased neurotransmitter release, resulting in a faster time to paralysis (Mahoney et al. 2006; Alfonso et al. 1993). Aldicarb resistance, on the

other hand, is consistent with decreased neurotransmitter release, and a longer time to paralysis (Mahoney et al. 2006; Alfonso et al. 1993).

We did not screen randomly mutagenized *C.elegans* individuals, but instead used a new approach enabled by the recent feasibility of the "million mutation project" - an affordable, large scale, whole genome sequencing project. This project sought to provide the *C. elegans* research community with pre-mapped mutants in every single protein-coding gene (Thompson et al. 2013). The mutagens utilized (EMS, ENU, or a cocktail of both) were selected to preferentially induce point mutations rather than significant deletions or large chromosomal aberrations (Thompson et al. 2013). Using the information provided by this study, we selected four different pre-mapped *C. elegans* strains, each with a missense mutation encoding a different allelic variation of the *vha-12* gene. We characterized the aldicarb sensitivity phenotypes of the following VC strains of interest: the *vha-12(gk629998)X* mutant VC40421 strain, the *vha-12(gk672728)X* mutant VC40512 strain, the *vha-12(gk277575)X* mutant VC40082 strain, and the *vha-12(gk879986)X* mutant VC40914 strain (Thompson et al. 2013). We suggest that significant differences in the aldicarb sensitivity phenotypes and survival probabilities between one or more of the VC strains and the control strains would be evidence in support of the pH model. Results from this study were, confounding, but appear to be consistent with the initial hypothesis that vesicle pH is a requirement for fusion.

Implications of VC40512 Results

Statistical analyses of the VC40512 data indicate there was no difference in the aldicarb sensitivity phenotype between wild-type (N2) and VC40512, suggesting that the *vha-12(gk672728)X* missense mutation affecting the V_1 B subunit of the V-ATPase is not related

to presynaptic defects with vesicle acidification. Although the survival probability for VC40512 was nonsignificant, we expected to see a range of phenotypes from the known genotypes, including some that may not have resulted in large enough molecular alterations to result in significant phenotypes. Additionally, my colleague Adya Agarwal, found no significant levamisole paralysis phenotype associated with this strain, indicating no postsynaptic effects in VC40512. These data suggest that the *vha-12* mutation in the VC40512 strain is phenotypically silent, which is consistent with the interpretation that some single-nucleotide missense mutations could potentially result in mild changes that have little effect on the V-ATPase's activity. There is also a possibility that a background mutation in this mutant's genome could have suppressed any change in *vha-12* activity. Ultimately, the aldicarb paralysis phenotype observed in this mutant provides no additional context on the status of our hypothesis.

Implications of VC40082 Results

Statistical analyses of VC40082 data indicate contradictory significance in the aldicarb sensitivity phenotypes between wild-type, MT7907, and VC40082. During one assay, the results showed that the survival probability of VC40082 was significantly higher than N2, whereas the remaining two assays indicated that the survival probability of VC40082 was significantly lower than wild-type. Because significance in survival probability for VC40082 was observed on both sides of the spectrum (resistance and hypersensitivity), our results are inconclusive. The variation in survival probability for VC40082 may have been caused by paralysis scoring errors and variations in population size (for this set of assays). Based on statistical results from the collapsed data set for this strain, it seems unlikely that a *vha-12(gk277575)X* missense mutation affecting the V_1 B subunit of the V-ATPase is related to presynaptic defects in the VC40082

strain. Regardless, we still cannot rule out the possibility that this strain may have a significant aldicarb paralysis phenotype. Interestingly, my colleague, Adya, found that the VC40082 strain exhibited a resistant levamisole paralysis phenotype compared to wild-type, suggesting that the effects of this V-ATPase mutation are localized to the postsynaptic cell. These postsynaptic effects may be a result of changes in cholinergic receptor expression on the postsynaptic membrane, however, this remains unclear. Some studies have already indicated the involvement of the V-ATPase through acidification in other endocytic pathways, such as the recruitment of small GTPase Arf6 and ARNO from the cytosol to endosomal membranes (Hurtado-Lorenzo et al. 2006). Although we suspect presynaptic effects of the *vha-12* mutation in the VC40082 strain to be phenotypically silent, and the resulting defects in neurotransmission to be localized to the postsynaptic cell, we cannot definitively rule out presynaptic effects due to inconclusive results. Additional aldicarb assay data for this mutant should be collected and reviewed to concretely verify (or reject) its overall lack of significant change in aldicarb sensitivity phenotype from wild-type. Ultimately, these data for the VC40082 mutant provide no information about the role of the V-ATPase and vesicle acidification in fusion competency. However, these data may point to potential postsynaptic roles of the V-ATPase in endocytic pathways related to receptor trafficking and recycling.

Implications of VC40421 Results

On the contrary, statistical analyses of VC40421 data indicate that the aldicarb sensitivity phenotype of VC40421 was hypersensitive compared to both the wild-type and resistant controls. Interestingly, my colleague Adya found this same strain to exhibit a hypersensitive levamisole paralysis phenotype, suggesting that this mutant also suffers from postsynaptic

defects. Despite evidence of postsynaptic deficiencies, this does not rule out the possibility for compounded presynaptic effects that could have been indicated by aldicarb paralysis phenotype. Any of these observations may have been caused by changes in receptor expression (as suggested for VC40082), amplification of pre- or postsynaptic receptor response, and changes in vesicle acidification via the V-ATPase. We suspect a portion of these defects in neurotransmission resulting from a *vha-12(gk629998)X* missense mutation affecting the V_1 B subunit of the V-ATPase to be localized both pre- and postsynaptically. If it is true that the VC40421 mutant exhibits a hypersensitive aldicarb sensitivity phenotype as a result of V-ATPase induced vesicle pH defects, this would provide strong support for the pH model hypothesis. Following studies should perform more specific experiments on the VC40421 mutants to identify or deny the presence of presynaptic defects related to V-ATPase synaptic vesicle acidification. Alternative studies may also aim to look at the role of the V-ATPase in receptor expression and endocytosis for this particular *C. elegans* mutant as well. Additionally, this evidence would strongly oppose the hypothesis for the function of the V-ATPase as suggested by the fusogen model. These conclusions are tentative, and require additional evidence to more concretely determine the implications indicated by the data.

Implications of VC40914 Results

Lastly, statistical analyses of VC40914 data indicate that the aldicarb sensitivity phenotype of this strain was mildly resistant compared to the wild-type control. However, for the first assay, it was observed that the survival probability for VC40914 was significantly less than the resistant control, and no different from the wild-type control, which directly contradicts the two following assays indicating exactly opposite results. It seems likely that VC40914 strain

exhibits mild resistance compared to the wild-type control, and that contradictory results from the first assay may be a result of scoring errors (however, this is still unclear). The collapsed data set indicates that the survival probability of VC40914 was, on average, greater than N2, but less than MT7907 across time points, suggesting that VC40914 exhibits a mild resistance (not as strongly as MT7907, yet still significant) in the presence of an aldicarb neurotoxin. It is possible that VC40914 exhibits stronger resistance than indicated, considering that the first assay could have skewed the data. Additionally, my colleague, Adya, observed a nonsignificant levamisole paralysis phenotype. It is probable that the *vha-12(gk879986)X* mutation affecting the V_1 B subunit of the V-ATPase proton pump is localized to the presynaptic cell. Furthermore, this suggests that these results are a product of acidification abnormalities due to V-ATPase V_1 sector dysfunction. These data support the pH model hypothesis, which proposes that the pH gradient generated by the V-ATPase proton pump acts as a quality-control checkpoint where only properly acidified vesicles fuse. Finally, these data are consistent with the overall predictions that we would expect a range of aldicarb paralysis phenotypes associated with different allelic variants. We had previously observed phenotypes no different from wild-type, a hypersensitive phenotype, and now a mildly resistant phenotype. This evidence strongly contradicts the hypothesis proposed by the fusogen model, which would not predict changes in the V_1 sector affecting vesicle acidification to result in changes in neurotransmission. Instead, it would predict that only changes made to the V_o sector would affect neurotransmission as a result of the physical association between the V-ATPase and the terminal plasma membrane to form a fusion pore.

Comparison of Body-Bending with Aldicarb Paralysis Phenotype

Interestingly, we found that the aldicarb paralysis phenotype reported in this study corresponds to the body-bending phenotype for VC40914, VC40421, and VC40082 reported by a previous thesis student, Dorjey Sherpa (VC40512 was not tested for a body-bending phenotype) (Ernstrom, personal communication). Sherpa found that both VC40421 and VC40914 exhibited decreased body-bends per minute when individuals were suspended in water, compared to wild-type. These findings correspond to significant locomotion defects associated with changes in synaptic transmission, which is consistent with the significant aldicarb paralysis phenotypes observed in both VC40421 and VC40512. Additionally, Sherpa did not see a difference in the average number of body-bends per minute in the VC40082 strain compared to wild-type, which is consistent with my results suggesting a nonsignificant aldicarb paralysis phenotype for this strain. Supplemental results from Dorjey Sherpa's study can be found in Appendix C.

MT7907 as a Resistant Control

We used the known *vha-12(n2915sd)X* partial loss-of-function mutant, MT7907, as a resistant control to compare phenotypes across VC strains with a known mutant of the same allelic series. Following data analysis, it appears that MT7907 did not consistently exhibit resistance compared to wild-type throughout the course of experimentation. For the VC40082 assays, the MT7907 control exhibited either the same or a lower probability of survival compared to wild-type across all three assays, which was different than expected. Additionally, MT7907 was found to be resistant for only one of the VC40421 and VC40512 assays, respectively. However, MT7907 performed as expected for all VC40914 assays. We believe

some of the contradictory results for the previously characterized resistant control may be related to variations in population size (only for the VC40082 assays) and paralysis scoring errors. I noticed that MT7907 had a tendency to habituate or exhibit very minimal movement in response to stimulation with a worm pick. My ability to notice these minute movements may have led to premature deaths, and thus trends in survival probability that conflict with the literature for this strain. My scoring ability likely improved as experimentation progressed, which may have been why MT7907 exhibited resistance in each of the VC40914 assays (which were the last assays conducted prior to data collection). If I were to repeat this experiment again having no experience with scoring worms for paralysis, I would use a strain exhibiting stronger resistance (such as CB189).

Sources of Variability

Following this study, we found various points of improvement based on potential sources of error that may have contributed to confounding results. Firstly, all phenotype scoring was conducted in a subjective manner. We attempted to minimize bias by ensuring the same person was scoring all assays. However, scoring was done visually, via a dissecting microscope, which is subject to human error. We attempted to reduce these scoring errors by defining paralysis as three consecutive, gentle pokes where the worm failed to produce movement in response. This had some drawbacks, because we found that it led to premature determination of paralysis for some strains, namely, MT7907. MT7907 is a strain that has obvious physiological defects, including limited body-bending and sluggish movements. Thus, it is a strain that already exhibits difficulties with normal motor control, even without the application of aldicarb. It could have been more difficult for MT7907 worms to generate a noticeable response following the

application of a neurotoxin. This is consistent with my observations (as mentioned previously) that some strains, MT7907 in particular, have a tendency to sensitize to gentle pokes with a worm pick. I found that a strong caress with a worm pick would initiate a response in MT7907, where they may have not responded to a gentle tap. Our definition for paralysis most likely led to premature determination of paralysis in the MT7907 strain in particular, and perhaps others. Even when these MT7907 mutants did respond, I learned that their range of motion was very limited. During many of the later time points of the assay, I found that MT7907 responses were so subtle that they could only be viewed under the highest magnification, which I had not been aware of for earlier experiments. These discrepancies associated with my scoring ability may have hindered other results, including those for the VC40082 strain, where the results were observed to be contradictory. However, learning associated with my scoring ability is reflected by the results for MT7907 survival probability for the VC40914 assays, which all indicate resistance most consistent with the literature.

Another major limitation was my ability to score all worms within the ten minute time interval. I set up a timer for each assay to help me track the time, however, I found that I sometimes ran over the ten minutes and continued to score worms for a certain strain after their time was already finished. This occurred because oftentimes, I had not yet scored each one of the observed worms before the time was finished. I found that I spent a lot of my time at earlier time intervals corralling worms back to the center of their copper rings. Unfortunately, the worms were more interested in fleeing the aldicarb plate and took little interest in the OP50 spotted in the middle of each copper ring. Worms that managed to escape their copper rings had to be censored so that data points between strains were not potentially confused. Ideally, each strain would have received their own plate to prevent unnecessary censoring, and more time between

strain scoring would have been given. Strains were staggered by three minutes, which means that I was really only given those three minutes to count and score up to 20 worms at one time. Another alternative would be to design a video program that automatically scores and counts all worms of a specific strain, which could minimize human error and subjective biases.

Some other possible, yet minor errors could have been factors such as room temperature and age of the aldicarb plate media. As mentioned previously, the Q_{10} for *C. elegans* is approximately ~2, which means that their growth rate increases or decreases by a factor of 2 for every 10˚C increase or decrease in temperature. All *C. elegans* strains were kept in a controlled laboratory environment, and to our knowledge, room temperature changed by (at most) no more than 2.8˚C. It is therefore unlikely that ambient temperature was a significant source of variability.

Depending on the age of the aldicarb plate used, some of the more "fresh" plates may have been more potent than aldicarb plates poured one month prior. However, we would still expect to observe similar trends between strains regardless of the minimal changes in the drug potency. We could not definitively associate a particular effect of plate age and drug potency. Through the course of this year-long study two batches of aldicarb plates were poured with aldicarb dissolved in the warm agar before it solidified. One batch was poured in October (2023) and one in January (2024). Inspecting my results, except for VC40421 which were conducted with the October plates, strains were tested on both batches of aldicarb plates and direction of aldicarb sensitivity of the controls was not obviously correlated with batch.

Survey of Background Mutations

Each of the VC strains contain roughly 300-400 background mutations. It is possible that one of these background mutations could have contributed to the phenotypes observed in one or more of the VC strains assayed. We performed a database search through the million mutant project website (http://genome.sfu.ca/mmp/) to identify known mutations affecting aldicarb paralysis phenotypes reported in each of the VC test strain genomes. The aldicarb resistant mutations that we searched for were: *vha-12*, *slo-1* (coding for a calcium-activated potassium channel), *egl-30* (coding for G-protein α), *tom-1* (coding for tomosyn), *dgk-1* (coding for diacylglycerol kinase theta), *aex-6* (coding for Rab GTPase), *rab-3*, *unc-10*, *snt-1* (coding for synaptotagmin), *unc-64* (coding for syntaxin), *snb-1* (coding for synaptobrevin), *ric-1*, and *goa-1* (coding for G-protein α) (Mahoney et al. 2006). VC40512, VC40082, and VC40914 were all free of mutations in these genes (Thompson et al. 2013). However, VC40421 was found to possess a *dgk-1(gk629984)X* mutation where guanine was replaced with adenine at nucleotide number 987637, resulting in an amino acid change of threonine to isoleucine (Thompson et al. 2013). Previous work indicates that *dgk-1* codes for diacylglycerol kinase (DGKQ), and its activity functions downstream in a serotonin signaling pathway that regulates locomotion and synaptic transmission (Kinshore et al. 2020; Nurrish et al. 1999). *C. elegans* with *dgk-1(sy428)X* mutations have been characterized to exhibit strong hypersensitivity in response to aldicarb (Mahoney, 2006). Thus, the *dgk-1(gk629984)X* mutation found in the VC40421 strain could be an alternative source of hypersensitivity observed in these mutants, however this is certainly not guaranteed because the *dgk-1(gk629984)X* mutation found in VC40421 is an allelic variant of the *dgk-1(sy428)X* mutation associated with hypersensitivity. There is still a likelihood that this mutation is silent. Additionally, VC40421 was also found to possess an *aex-6(gk629427)I*

mutation where guanine was also replaced with adenine at nucleotide number 13543447, resulting in an amino acid exchange of arginine for cysteine (Thompson et al. 2013). *C. elegans* with *aex-6(sa24)I* mutations have been characterized to exhibit very mild resistance in response to aldicarb (Mahoney, 2006), which is inconsistent with the strong hypersensitivity in VC40421 mutants containing a background mutation in *aex-6(gk629427)I.* However, until this mutation is isolated, a role for *aex-6* in VC40421 hypersensitivity cannot be ruled out.

I also searched for other V-ATPase mutations that may be in the background of the strains we tested, which includes: *vha-1* through *vha-20*, *spe-5*, and *unc-32*. All strains except for VC40512 (a strain that did not have a statistically significant aldicarb phenotype different from wild-type), do not have any other mutations in *C. elegans* V-ATPase subunit genes. VC40512 had a *vha-15(gk273116)* missense mutation in the V_1 H subunit ortholog, resulting in a T187I amino acid change.

Mapping VC Strain Amino Acid Changes

I analyzed the primary structure of the VHA-12 sequence (found in Appendix D) with respect to conserved amino acid positions to determine if any of the mutations in the VC strains were near critical ATP catalytic sites. The V-ATPase B subunits contain two universally conserved amino acids across all *vha-12* orthologs in their sequence; an arginine at position 379 and a tyrosine at position 351, which correspond to the ATP binding site on the B subunit (Ernstrom et al. 2012). We found that the glutamate to lysine change exhibited in VC40512, was 54 amino acids away from arginine and 82 amino acids away from tyrosine (Ernstrom et al. 2012). The glutamate at position 433 was indicated to be heavily conserved in the *C. elegans* genome (Ernstrom et al. 2012). Perhaps this amino acid change was too distant from the ATP

binding site to exhibit effects, as evident from the VC40512 aldicarb paralysis phenotype. Alternatively, we found that the serine to phenylalanine change exhibited in VC40082 was more proximal to the ATP binding site. This change was 17 amino acids away from arginine, and 45 amino acids away from tyrosine (Ernstrom et al. 2012). However, the serine at position 396 was not indicated to be a conserved sequence in the *C. elegans* genome (Ernstrom et al. 2012), which may be the cause for the (tentative) lack of aldicarb paralysis phenotype observed in these mutants. Surprisingly, the isoleucine to leucine switch exhibited in VC40421 mutants was more distant from the ATP binding site, being 130 positions away from arginine and 102 positions away from tyrosine (Ernstrom et al. 2012). The isoleucine at position 249 was also highly conserved (Ernstrom et al. 2012). It is unclear how this conservative switch could have caused such a drastic phenotype in VC40421. Perhaps this is a result of high sequence conservation, however, it may be more effective to model these changes computationally. Finally, the glutamate to lysine amino acid change observed in the VC40914 mutants was indicated 102 positions away from arginine, and 130 positions away from tyrosine (Ernstrom et al. 2012). The glutamate at position 481 was not a highly conserved protein (Ernstrom et al. 2012). It is unclear why VC40914 and VC40421 exhibited more drastic aldicarb sensitivity phenotypes despite their amino acid changes being more obscured from the ATP binding site than both VC40082 and VC40512. These effects could be attributed to changes in highly conserved sequences or minor anatomical changes that have significant B subunit conformation effects. Future studies should model these anatomical changes to see how they might affect V-ATPase B subunit function.

Future Paths

Although these findings do not provide definitive answers, they may hint at the true mechanism(s) of the V-ATPase. There are many future directions that this study could lead to. A recommended first study would be an outcross for each of the VC strains used in this study. If one were to perform an outcross in a future experiment, they would first need to cultivate a healthy population of mutant strain male and wild-type female *C. elegans* nematodes (Anderson et al. 2020). Next, L4 mutant male and the wild-type female nematodes would be transferred to the same NGM plate to initiate mating, which would take place over the course of several hours. Once the eggs have been laid, adults would be removed from the plates. Outcrossing should be performed with males from each successive generation and wild-type females to clean up the background (however some background mutations may remain even after various rounds of outcrossing) (Anderson et al. 2020). DNA sequencing should be performed following the outcross to ensure that the mutation of interest remains while the seven characterized gene mutations affecting aldicarb paralysis phenotype listed previously, are absent. Other possible future routes include investigating mechanisms related to how the vesicle senses pH, the role of V-ATPases in receptor-mediated endocytic pathways, how clathrin mediated receptor endocytosis is altered in VC strains compared to wild-types strains, and performing direct in vivo measurements of how vesicle size and fusion frequency are altered in the previously tested VC mutants. This last route in particular can be achieved using electrophysiological methods similar to those initially conducted by del Castillo and Katz in 1954.

Conclusion

Ultimately, we assayed and characterized four *vha-12* mutant strains with unidentified aldicarb paralysis phenotypes in order to determine the role of V-ATPase mediated vesicle acidification in vesicle fusion. We found that the VC40082 (tentative) and VC40512 strains did not exhibit a significant phenotype, whereas, the VC40421 strain was hypersensitive, and the VC40914 strain was mildly resistant. These data establish a clear experimental path to further investigate how these mutations alter aldicarb sensitivity and possibly contribute to acidification-dependent vesicle fusion competency.

Literature Cited

Alfonso A, Grundahl K, Duerr JS, Han HP, Rand JB. The *Caenorhabditis elegans unc-17* gene: a putative vesicular acetylcholine transporter. Science. 1993;261(5121):617-9. Epub 1993/07/30. doi: 10.1126/science.8342028. PubMed PMID: 8342028.

Anderson JL, Morran LT, Phillips PC. Outcrossing and the maintenance of males within *C. elegans* populations. J Hered. 2010;101 Suppl 1(Suppl 1):S62-74. Epub 2010/03/10. doi: 10.1093/jhered/esq003. PubMed PMID: 20212008; PubMed Central PMCID: PMCPMC2859890.

Anne C, Gasnier B. Vesicular neurotransmitter transporters: mechanistic aspects. Curr Top Membr. 2014;73:149-74. Epub 2014/04/22. doi: 10.1016/b978-0-12-800223-0.00003-7. PubMed PMID: 24745982.

Axelrod J. Catecholamine neurotransmitters, psychoactive drugs, and biological clocks. J Neurosurg. 1981;55(5): 669-77.

Bessereau JL. Insertional mutagenesis in *C. elegans* using the Drosophila transposon *Mos1*: a method for the rapid identification of mutated genes. Methods Mol Biol. 2006;351:59-73. Epub 2006/09/22. doi: 10.1385/1-59745-151-7:59. PubMed PMID: 16988426.

Beyenbach KW, Wieczorek H. The V-type H^+-ATPase: molecular structure and function, physiological roles and regulation. J Exp Biol. 2006;209(Pt 4):577-89. Epub 2006/02/02. doi: 10.1242/jeb.02014. PubMed PMID: 16449553.

Bodzęta A, Kahms M, Klingauf J. The Presynaptic v-ATPase reversibly disassembles and thereby modulates exocytosis but is not part of the fusion machinery. Cell Rep. 2017;20(6):1348-59. Epub 2017/08/10. doi: 10.1016/j.celrep.2017.07.040. PubMed PMID: 28793259.

Bowman BJ, Vázquez-Laslop N, Bowman EJ. The vacuolar ATPase of *Neurospora crassa*. J Bioenerg Biomembr. 1992;24(4):361-70. Epub 1992/08/01. doi: 10.1007/bf00762529. PubMed PMID: 1400281.

Brenner S. The genetics of *Caenorhabditis elegans*. Genetics. 1974;77(1):71-94. Epub 1974/05/01. doi: 10.1093/genetics/77.1.71. PubMed PMID: 4366476; PubMed Central PMCID: PMCPMC1213120.

Brown D, Paunescu TG, Breton S, Marshansky V. Regulation of the V-ATPase in kidney epithelial cells: dual role in acid–base homeostasis and vesicle trafficking. J Exp Biol. 2009;212(11):1762-72. doi: 10.1242/jeb.028803.

Caire MJ, Reddy V, Varacallo M. Physiology, Synapse. 2023 Mar 27. In: StatPearls [Internet]. Treasure Island (FL): StatPearls Publishing; 2024 Jan. PMID: 30252303.

Changeux JP. Discovery of the first neurotransmitter receptor: the acetylcholine nicotinic receptor. Biomolecules. 2020;10(4). Epub 2020/04/09. doi: 10.3390/biom10040547. PubMed PMID: 32260196; PubMed Central PMCID: PMCPMC7226243.

Corsi AK, Wightman B, Chalfie M. A Transparent Window into Biology: A Primer on *Caenorhabditis elegans*. Genetics. 2015;200(2):387-407. doi: 10.1534/genetics.115.176099.

Cousin MA, Nicholls DG. Synaptic vesicle recycling in cultured cerebellar granule cells: role of vesicular acidification and refilling. J Neurochem. 1997;69(5):1927-35. Epub 1998/02/12. doi: 10.1046/j.1471-4159.1997.69051927.x. PubMed PMID: 9349537.

Croft BG, Fortin GD, Corera AT, Edwards RH, Beaudet A, Trudeau LE, et al. Normal biogenesis and cycling of empty synaptic vesicles in dopamine neurons of vesicular monoamine transporter 2 knockout mice. Mol Biol Cell. 2005;16(1):306-15. Epub 2004/10/22. doi: 10.1091/mbc.e04-07-0559. PubMed PMID: 15496457; PubMed Central PMCID: PMCPMC539174.

Crouse WL, Kelada SNP, Valdar W. Inferring the allelic series at QTL in multiparental populations. Genetics. 2020;216(4):957-83. Epub 2020/10/22. doi: 10.1534/genetics.120.303393. PubMed PMID: 33082282; PubMed Central PMCID: PMCPMC7768242.

Davis MW, Hammarlund M, Harrach T, Hullett P, Olsen S, Jorgensen EM. Rapid single nucleotide polymorphism mapping in *C. elegans*. BMC Genomics. 2005;6(1):118. doi: 10.1186/1471-2164-6-118.

de Castro BM, Pereira GS, Magalhães V, Rossato JI, De Jaeger X, Martins-Silva C, et al. Reduced expression of the vesicular acetylcholine transporter causes learning deficits in mice. Genes Brain Behav. 2009;8(1):23-35. Epub 2008/09/10. doi: 10.1111/j.1601-183X.2008.00439.x. PubMed PMID: 18778400.

Del Castillo J, Katz B. Quantal components of the end-plate potential. J Physiol. 1954;124(3):560-73. Epub 1954/06/28. doi: 10.1113/jphysiol.1954.sp005129. PubMed PMID: 13175199; PubMed Central PMCID: PMCPMC1366292.

Eastman C, Horvitz HR, Jin Y. Coordinated transcriptional regulation of the *unc-25* glutamic acid decarboxylase and the unc-47 GABA vesicular transporter by the *Caenorhabditis elegans* UNC-30 homeodomain protein. J Neurosci. 1999;19(15):6225-34. Epub 1999/07/22. doi: 10.1523/jneurosci.19-15-06225.1999. PubMed PMID: 10414952; PubMed Central PMCID: PMCPMC6782798.

Eaton AF, Merkulova M, Brown D. The H(+)-ATPase (V-ATPase): from proton pump to signaling complex in health and disease. Am J Physiol Cell Physiol. 2021;320(3):C392-c414. Epub 2020/12/17. doi: 10.1152/ajpcell.00442.2020. PubMed PMID: 33326313; PubMed Central PMCID: PMCPMC8294626.

Edwards RH. The neurotransmitter cycle and quantal size. Neuron. 2007;55(6):835-58. Epub 2007/09/21. doi: 10.1016/j.neuron.2007.09.001. PubMed PMID: 17880890.

Edwards RH. The neurotransmitter cycle and quantal size. Neuron. 2007;55(6):835-58. Epub 2007/09/21. doi: 10.1016/j.neuron.2007.09.001. PubMed PMID: 17880890.

El Far O, Seagar M. A role for V-ATPase subunits in synaptic vesicle fusion? J Neurochem. 2011;117(4):603-12. Epub 2011/03/08. doi: 10.1111/j.1471-4159.2011.07234.x. PubMed PMID: 21375531.

Ernstrom GG, Weimer R, Pawar DR, Watanabe S, Hobson RJ, Greenstein D, et al. V-ATPase V_1 sector is required for corpse clearance and neurotransmission in *Caenorhabditis elegans*. Genetics. 2012;191(2):461-75. Epub 2012/03/20. doi: 10.1534/genetics.112.139667. PubMed PMID: 22426883; PubMed Central PMCID: PMCPMC3374311.

Fatt P, Katz B. An analysis of the end-plate potential recorded with an intracellular electrode. J Physiol. 1951;115(3):320-70. Epub 1951/11/28. doi: 10.1113/jphysiol.1951.sp004675. PubMed PMID: 14898516; PubMed Central PMCID: PMCPMC1392060.

Fay D, Bender A. SNPs: introduction and two-point mapping. WormBook. 2008:1-10. Epub 2008/09/27. doi: 10.1895/wormbook.1.93.2. PubMed PMID: 18819170; PubMed Central PMCID: PMCPMC10083728.

Fire A, Xu S, Montgomery MK, Kostas SA, Driver SE, Mello CC. Potent and specific genetic interference by double-stranded RNA in *Caenorhabditis elegans*. Nature. 1998;391(6669):806-11. Epub 1998/03/05. doi: 10.1038/35888. PubMed PMID: 9486653.

Forgac M. Vacuolar ATPases: rotary proton pumps in physiology and pathophysiology. Nature Reviews Molecular Cell Biology. 2007;8(11):917-29. doi: 10.1038/nrm2272.

Francis MM, Maricq AV. Electrophysiological analysis of neuronal and muscle function in *C. elegans*. Methods Mol Biol. 2006;351:175-92. Epub 2006/09/22. doi: 10.1385/1-59745-151-7:175. PubMed PMID: 16988434.

Frattini A, Orchard PJ, Sobacchi C, Giliani S, Abinun M, Mattsson JP, et al. Defects in TCIRG1 subunit of the vacuolar proton pump are responsible for a subset of human autosomal recessive osteopetrosis. Nature Genetics. 2000;25(3):343-6. doi: 10.1038/77131.

Futerman AH, van Meer G. The cell biology of lysosomal storage disorders. Nat Rev Mol Cell Biol. 2004;5(7):554-65. Epub 2004/07/03. doi: 10.1038/nrm1423. PubMed PMID: 15232573.

Golden JW, Riddle DL. The *Caenorhabditis elegans* dauer larva: developmental effects of pheromone, food, and temperature. Dev Biol. 1984;102(2):368-78. Epub 1984/04/01. doi: 10.1016/0012-1606(84)90201-x. PubMed PMID: 6706004.

Goodman MB, Hall DH, Avery L, Lockery SR. Active currents regulate sensitivity and dynamic range in C. elegans neurons. Neuron. 1998;20(4):763-72. Epub 1998/05/15. doi: 10.1016/s0896-6273(00)81014-4. PubMed PMID: 9581767; PubMed Central PMCID: PMCPMC4444786.

Grant BD, Sato M. Intracellular trafficking. WormBook. 2006:1-9. Epub 2007/12/01. doi: 10.1895/wormbook.1.77.1. PubMed PMID: 18050485; PubMed Central PMCID: PMCPMC4781316.

Hahn H, Kang HG, Ha IS, Cheong HI, Choi Y. ATP6B1 gene mutations associated with distal renal tubular acidosis and deafness in a child. Am J Kidney Dis. 2003;41(1):238-43. Epub 2002/12/25. doi: 10.1053/ajkd.2003.50014. PubMed PMID: 12500243.

Hardy S, Legagneux V, Audic Y, Paillard L. Reverse genetics in eukaryotes. Biol Cell. 2010;102(10):561-80. Epub 2010/09/04. doi: 10.1042/bc20100038. PubMed PMID: 20812916; PubMed Central PMCID: PMCPMC3017359.

Hiesinger PR, Fayyazuddin A, Mehta SQ, Rosenmund T, Schulze KL, Zhai RG, et al. The v-ATPase V0 subunit a1 is required for a late step in synaptic vesicle exocytosis in *Drosophila*. Cell. 2005;121(4):607-20. Epub 2005/05/24. doi: 10.1016/j.cell.2005.03.012. PubMed PMID: 15907473; PubMed Central PMCID: PMCPMC3351201.

Hobert O. The neuronal genome of *Caenorhabditis elegans*. WormBook. 2013:1-106. Epub 2013/10/02. doi: 10.1895/wormbook.1.161.1. PubMed PMID: 24081909; PubMed Central PMCID: PMCPMC4781646.

Hurtado-Lorenzo A, Skinner M, Annan JE, Futai M, Sun-Wada G-H, Bourgoin S, et al. V-ATPase interacts with ARNO and Arf6 in early endosomes and regulates the protein degradative pathway. Nature Cell Biology. 2006;8(2):124-36. doi: 10.1038/ncb1348.

Hyman SE. Neurotransmitters. Curr Biol. 2005;15(5):R154-8. Epub 2005/03/09. doi: 10.1016/j.cub.2005.02.037. PubMed PMID: 15753022.

Iversen L. Neurotransmitter transporters and their impact on the development of psychopharmacology. Br J Pharmacol. 2006;147 Suppl 1(Suppl 1):S82-8. Epub 2006/01/13. doi: 10.1038/sj.bjp.0706428. PubMed PMID: 16402124; PubMed Central PMCID: PMCPMC1760736.

Jabeen S, Thirumalai V. The interplay between electrical and chemical synaptogenesis. J Neurophysiol. 2018;120(4):1914-22. Epub 2018/08/02. doi: 10.1152/jn.00398.2018. PubMed PMID: 30067121; PubMed Central PMCID: PMCPMC6230774.

Jahn R, Südhof TC. Membrane fusion and exocytosis. Annu Rev Biochem. 1999;68:863-911. Epub 2000/06/29. doi: 10.1146/annurev.biochem.68.1.863. PubMed PMID: 10872468.

Karet FE, Finberg KE, Nelson RD, Nayir A, Mocan H, Sanjad SA, et al. Mutations in the gene encoding B1 subunit of H^+-ATPase cause renal tubular acidosis with sensorineural deafness. Nat Genet. 1999;21(1):84-90. Epub 1999/01/23. doi: 10.1038/5022. PubMed PMID: 9916796.

Katz B. The release of neural transmitter substances. Liverpool: Liverpool University Press; 1969.

Kishore R, Arnaboldi V, Van Slyke CE, Chan J, Nash RS, Urbano JM, et al. Automated generation of gene summaries at the Alliance of Genome Resources. Database. 2020;2020. doi: 10.1093/database/baaa037.

Konopka RJ, Benzer S. Clock mutants of *Drosophila melanogaster*. Proc Natl Acad Sci U S A. 1971;68(9):2112-6. Epub 1971/09/01. doi: 10.1073/pnas.68.9.2112. PubMed PMID: 5002428; PubMed Central PMCID: PMCPMC389363.

Lee S-K, Li W, Ryu S-E, Rhim T, Ahnn J. Vacuolar H+-ATPases in *Caenorhabditis elegans*: What can we learn about giant H^+ pumps from tiny worms? Biochimica et Biophysica Acta (BBA) - Bioenergetics. 2010;1797(10):1687-95. doi: https://doi.org/10.1016/j.bbabio.2010.07.004.

Levitan IB, Kaczmarek LK. The neuron : cell and molecular biology. Fourth edition. ed. Oxford ; New York: Oxford University Press; 2015. xvi, 579 pages.

Liégeois S, Benedetto A, Garnier JM, Schwab Y, Labouesse M. The V0-ATPase mediates apical secretion of exosomes containing Hedgehog-related proteins in *Caenorhabditis elegans*. J Cell Biol. 2006;173(6):949-61. Epub 2006/06/21. doi: 10.1083/jcb.200511072. PubMed PMID: 16785323; PubMed Central PMCID: PMCPMC2063919.

Lima Rde F, Prado VF, Prado MA, Kushmerick C. Quantal release of acetylcholine in mice with reduced levels of the vesicular acetylcholine transporter. J Neurochem. 2010;113(4):943-51. Epub 2010/03/06. doi: 10.1111/j.1471-4159.2010.06657.x. PubMed PMID: 20202084; PubMed Central PMCID: PMCPMC2866190.

López-Corcuera B, Geerlings A, Aragón C. Glycine neurotransmitter transporters: an update. Mol Membr Biol. 2001;18(1):13-20. Epub 2001/06/09. PubMed PMID: 11396606.

Lu M, Ammar D, Ives H, Albrecht F, Gluck SL. Physical interaction between aldolase and vacuolar H^+-ATPase is essential for the assembly and activity of the proton pump. J Biol Chem. 2007;282(34):24495-503. Epub 2007/06/20. doi: 10.1074/jbc.M702598200. PubMed PMID: 17576770.

Lu M, Holliday LS, Zhang L, Dunn WA, Jr., Gluck SL. Interaction between aldolase and vacuolar H+-ATPase: evidence for direct coupling of glycolysis to the ATP-hydrolyzing proton pump. J Biol Chem. 2001;276(32):30407-13. Epub 2001/06/16. doi: 10.1074/jbc.M008768200. PubMed PMID: 11399750.

Lu M, Sautin YY, Holliday LS, Gluck SL. The glycolytic enzyme aldolase mediates assembly, expression, and activity of vacuolar H+-ATPase. J Biol Chem. 2004;279(10):8732-9. Epub 2003/12/16. doi: 10.1074/jbc.M303871200. PubMed PMID: 14672945.

Mahoney TR, Luo S, Nonet ML. Analysis of synaptic transmission in *Caenorhabditis elegans* using an aldicarb-sensitivity assay. Nat Protoc. 2006;1(4):1772-7. Epub 2007/05/10. doi: 10.1038/nprot.2006.281. PubMed PMID: 17487159.

Marshansky V. The V-ATPase a2-subunit as a putative endosomal pH-sensor. Biochem Soc Trans. 2007;35(Pt 5):1092-9. Epub 2007/10/25. doi: 10.1042/bst0351092. PubMed PMID: 17956287.

Mauvezin C, Neufeld TP. Bafilomycin A1 disrupts autophagic flux by inhibiting both V-ATPase-dependent acidification and Ca-P60A/SERCA-dependent autophagosome-lysosome fusion. Autophagy. 2015;11(8):1437-8. Epub 2015/07/15. doi: 10.1080/15548627.2015.1066957. PubMed PMID: 26156798; PubMed Central PMCID: PMCPMC4590655.

McIntire SL, Reimer RJ, Schuske K, Edwards RH, Jorgensen EM. Identification and characterization of the vesicular GABA transporter. Nature. 1997;389(6653):870-6. Epub 1997/12/31 23:16. doi: 10.1038/39908. PubMed PMID: 9349821.

McIntire SL, Jorgensen E, Horvitz HR. Genes required for GABA function in *Caenorhabditis elegans*. Nature. 1993;364(6435):334-7. doi: 10.1038/364334a0.

Meldrum BS. Glutamate as a neurotransmitter in the brain: review of physiology and pathology. J Nutr. 2000;130(4S Suppl):1007s-15s. Epub 2000/03/29. doi: 10.1093/jn/130.4.1007S. PubMed PMID: 10736372.

Miesenböck G, De Angelis DA, Rothman JE. Visualizing secretion and synaptic transmission with pH-sensitive green fluorescent proteins. Nature. 1998;394(6689):192-5. doi: 10.1038/28190.

Miller KG, Alfonso A, Nguyen M, Crowell JA, Johnson CD, Rand JB. A genetic selection for *Caenorhabditis elegans* synaptic transmission mutants. Proc Natl Acad Sci U S A. 1996;93(22):12593-8. Epub 1996/10/29. doi: 10.1073/pnas.93.22.12593. PubMed PMID: 8901627; PubMed Central PMCID: PMCPMC38037.

Miller MW. GABA as a Neurotransmitter in Gastropod Molluscs. Biol Bull. 2019;236(2):144-56. Epub 2019/04/02. doi: 10.1086/701377. PubMed PMID: 30933636; PubMed Central PMCID: PMCPMC7710352.

Moechars D, Weston MC, Leo S, Callaerts-Vegh Z, Goris I, Daneels G, et al. Vesicular glutamate transporter VGLUT2 expression levels control quantal size and neuropathic pain. J Neurosci. 2006;26(46):12055-66. Epub 2006/11/17. doi: 10.1523/jneurosci.2556-06.2006. PubMed PMID: 17108179; PubMed Central PMCID: PMCPMC6674853.

Moerman DG, Fire A. Muscle: Structure, Function, and Development. In: Riddle DL, Blumenthal T, Meyer BJ, Priess JR, editors. C elegans II. 2nd ed. Cold Spring Harbor (NY)1997.

Morel N, Dedieu JC, Philippe JM. Specific sorting of the a1 isoform of the V-H+ATPase a subunit to nerve terminals where it associates with both synaptic vesicles and the presynaptic plasma membrane. J Cell Sci. 2003;116(Pt 23):4751-62. Epub 2003/11/06. doi: 10.1242/jcs.00791. PubMed PMID: 14600261.

Moriyama Y, Nelson N. The purified ATPase from chromaffin granule membranes is an anion-dependent proton pump. J Biol Chem. 1987;262(19):9175-80. Epub 1987/07/05. PubMed PMID: 2885327.

Nurrish S, Ségalat L, Kaplan JM. Serotonin inhibition of synaptic transmission: $G_{\alpha o}$ Decreases the abundance of UNC-13 at release sites. Neuron. 1999;24(1):231-42. doi: https://doi.org/10.1016/S0896-6273(00)80835-1.

Oh KH, Kim H. Aldicarb-induced paralysis assay to determine defects in synaptic transmission in *Caenorhabditis elegans*. Bio Protoc. 2017;7(14). Epub 2017/09/05. doi: 10.21769/BioProtoc.2400. PubMed PMID: 28868330; PubMed Central PMCID: PMCPMC5580937.

Oikonomou G, Shaham S. The glia of *Caenorhabditis elegans*. Glia. 2011;59(9):1253-63. Epub 2011/07/07. doi: 10.1002/glia.21084. PubMed PMID: 21732423; PubMed Central PMCID: PMCPMC3117073.

Omote H, Moriyama Y. Vesicular neurotransmitter transporters: an approach for studying transporters with purified proteins. Physiology (Bethesda). 2013;28(1):39-50. Epub 2013/01/03. doi: 10.1152/physiol.00033.2012. PubMed PMID: 23280356.

Parsons RL, Calupca MA, Merriam LA, Prior C. Empty synaptic vesicles recycle and undergo exocytosis at vesamicol-treated motor nerve terminals. J Neurophysiol. 1999;81(6):2696-700. Epub 1999/06/16. doi: 10.1152/jn.1999.81.6.2696. PubMed PMID: 10368389.

Peters C, Bayer MJ, Bühler S, Andersen JS, Mann M, Mayer A. Trans-complex formation by proteolipid channels in the terminal phase of membrane fusion. Nature. 2001;409(6820):581-8. Epub 2001/02/24. doi: 10.1038/35054500. PubMed PMID: 11214310.

Platt FM, Boland B, van der Spoel AC. The cell biology of disease: lysosomal storage disorders: the cellular impact of lysosomal dysfunction. J Cell Biol. 2012;199(5):723-34. Epub 2012/11/28. doi: 10.1083/jcb.201208152. PubMed PMID: 23185029; PubMed Central PMCID: PMCPMC3514785.

Poëa-Guyon S, Ammar MR, Erard M, Amar M, Moreau AW, Fossier P, et al. The V-ATPase membrane domain is a sensor of granular pH that controls the exocytotic machinery. J Cell Biol. 2013;203(2):283-98. Epub 2013/10/30. doi: 10.1083/jcb.201303104. PubMed PMID: 24165939; PubMed Central PMCID: PMCPMC3812966.

Pothos EN, Larsen KE, Krantz DE, Liu Y, Haycock JW, Setlik W, et al. Synaptic vesicle transporter expression regulates vesicle phenotype and quantal size. J Neurosci. 2000;20(19):7297-306. Epub 2000/09/29. doi: 10.1523/jneurosci.20-19-07297.2000. PubMed PMID: 11007887; PubMed Central PMCID: PMCPMC6772799.

Prado VF, Martins-Silva C, de Castro BM, Lima RF, Barros DM, Amaral E, et al. Mice deficient for the vesicular acetylcholine transporter are myasthenic and have deficits in object and social recognition. Neuron. 2006;51(5):601-12. Epub 2006/09/05. doi: 10.1016/j.neuron.2006.08.005. PubMed PMID: 16950158.

Raizen DM, Zimmerman JE, Maycock MH, Ta UD, You YJ, Sundaram MV, et al. Lethargus is a *Caenorhabditis elegans* sleep-like state. Nature. 2008;451(7178):569-72. Epub 2008/01/11. doi: 10.1038/nature06535. PubMed PMID: 18185515.

Rand JB, Duerr JS, Frisby DL. Neurogenetics of vesicular transporters in *C. elegans*. Faseb j. 2000;14(15):2414-22. Epub 2000/12/02. doi: 10.1096/fj.00-0313rev. PubMed PMID: 11099459.

Rost BR, Schneider F, Grauel MK, Wozny C, Bentz C, Blessing A, et al. Optogenetic acidification of synaptic vesicles and lysosomes. Nat Neurosci. 2015;18(12):1845-52. Epub 2015/11/10. doi: 10.1038/nn.4161. PubMed PMID: 26551543; PubMed Central PMCID: PMCPMC4869830.

Sam C, Bordoni B. Physiology, Acetylcholine. 2023 Apr 10. In: StatPearls [Internet]. Treasure Island (FL): StatPearls Publishing; 2024 Jan. 2023 Apr 10. PMID: 32491757

Sankaranarayanan S, Ryan TA. Real-time measurements of vesicle-SNARE recycling in synapses of the central nervous system. Nature Cell Biology. 2000;2(4):197-204. doi: 10.1038/35008615.

Sankaranarayanan S, Ryan TA. CHAPTER 6 - Neuronal Exocytosis. In: Bean AJ, editor. Protein Trafficking in Neurons. Burlington: Academic Press; 2007. p. 97-124.

Seol JH, Shevchenko A, Shevchenko A, Deshaies RJ. Skp1 forms multiple protein complexes, including RAVE, a regulator of V-ATPase assembly. Nat Cell Biol. 2001;3(4):384-91. Epub 2001/04/03. doi: 10.1038/35070067. PubMed PMID: 11283612.

Shechter E. Secondary active transport. Biochimie. 1986;68(3):357-65. Epub 1986/03/01. doi: 10.1016/s0300-9084(86)80002-5. PubMed PMID: 3017449.

Song H, Ming G, Fon E, Bellocchio E, Edwards RH, Poo M. Expression of a putative vesicular acetylcholine transporter facilitates quantal transmitter packaging. Neuron. 1997;18(5):815-26. Epub 1997/05/01. doi: 10.1016/s0896-6273(00)80320-7. PubMed PMID: 9182805.

Song Q, Meng B, Xu H, Mao Z. The emerging roles of vacuolar-type ATPase-dependent Lysosomal acidification in neurodegenerative diseases. Transl Neurodegener. 2020;9(1):17. Epub 2020/05/13. doi: 10.1186/s40035-020-00196-0. PubMed PMID: 32393395; PubMed Central PMCID: PMCPMC7212675.

Starich T, Sheehan M, Jadrich J, Shaw J. Innexins in *C. elegans*. Cell Commun Adhes. 2001;8(4-6):311-4. Epub 2002/06/18. doi: 10.3109/15419060109080744. PubMed PMID: 12064609.

Stevens TH, Forgac M. Structure, function and regulation of the vacuolar (H+)-ATPase. Annu Rev Cell Dev Biol. 1997;13:779-808. Epub 1997/01/01. doi: 10.1146/annurev.cellbio.13.1.779. PubMed PMID: 9442887.

Stiernagle T. Maintenance of *C. elegans*. WormBook. 2006:1-11. Epub 2007/12/01. doi: 10.1895/wormbook.1.101.1. PubMed PMID: 18050451; PubMed Central PMCID: PMCPMC4781397.

Südhof TC. Neurotransmitter release: the last millisecond in the life of a synaptic vesicle. Neuron. 2013;80(3):675-90. Epub 2013/11/05. doi: 10.1016/j.neuron.2013.10.022. PubMed PMID: 24183019; PubMed Central PMCID: PMCPMC3866025.

Sulston J, Hodgkin J. Methods in the nematode *C. elegans*. New York: Cold Spring Harbor Laboratory. 1988:587-606.

Takamori S. Presynaptic Molecular Determinants of Quantal Size. Front Synaptic Neurosci. 2016;8:2. Epub 2016/02/24. doi: 10.3389/fnsyn.2016.00002. PubMed PMID: 26903855; PubMed Central PMCID: PMCPMC4744840.

Thompson O, Edgley M, Strasbourger P, Flibotte S, Ewing B, Adair R, et al. The million mutation project: a new approach to genetics in *Caenorhabditis elegans*. Genome Res. 2013;23(10):1749-62. Epub 2013/06/27. doi: 10.1101/gr.157651.113. PubMed PMID: 23800452; PubMed Central PMCID: PMCPMC3787271.

Toei M, Saum R, Forgac M. Regulation and isoform function of the V-ATPases. Biochemistry. 2010;49(23):4715-23. doi: 10.1021/bi100397s.

Ungermann C, Wickner W, Xu Z. Vacuole acidification is required for trans-SNARE pairing, LMA1 release, and homotypic fusion. Proceedings of the National Academy of Sciences. 1999;96(20):11194-9. doi: doi:10.1073/pnas.96.20.11194.

von Euler US. Adrenergic neurotransmitter functions. Science. 1971;173(3993):202-6. Epub 1971/07/16. doi: 10.1126/science.173.3993.202. PubMed PMID: 4103433.

White JG, Southgate E, Thomson JN, Brenner S. The structure of the nervous system of the nematode *Caenorhabditis elegans*. Philos Trans R Soc Lond B Biol Sci. 1986;314(1165):1-340. Epub 1986/11/12. doi: 10.1098/rstb.1986.0056. PubMed PMID: 22462104.

Williams BD, Schrank B, Huynh C, Shownkeen R, Waterston RH. A genetic mapping system in *Caenorhabditis elegans* based on polymorphic sequence-tagged sites. Genetics. 1992;131(3):609-24. Epub 1992/07/01. doi: 10.1093/genetics/131.3.609. PubMed PMID: 1321065; PubMed Central PMCID: PMCPMC1205034.

Wojcik SM, Rhee JS, Herzog E, Sigler A, Jahn R, Takamori S, et al. An essential role for vesicular glutamate transporter 1 (VGLUT1) in postnatal development and control of quantal size. Proc Natl Acad Sci U S A. 2004;101(18):7158-63. Epub 2004/04/23. doi: 10.1073/pnas.0401764101. PubMed PMID: 15103023; PubMed Central PMCID: PMCPMC406482.

Wright KA. The Nematode's Cuticle: Its Surface and the Epidermis: Function, Homology, Analogy: A Current Consensus. The Journal of Parasitology. 1987;73(6):1077-83. doi: 10.2307/3282284.

Zarkower D. Somatic sex determination. WormBook. 2006:1-12. Epub 2007/12/01. doi: 10.1895/wormbook.1.84.1. PubMed PMID: 18050479; PubMed Central PMCID: PMCPMC4781091.

Zhou Q, Petersen CC, Nicoll RA. Effects of reduced vesicular filling on synaptic transmission in rat hippocampal neurons. J Physiol. 2000;525 Pt 1(Pt 1):195-206. Epub 2000/05/16. doi: 10.1111/j.1469-7793.2000.t01-1-00195.x. PubMed PMID: 10811737; PubMed Central PMCID: PMCPMC2269926.

Appendix A

Aldicarb Assay Statistical Results Tables

Table A1. *P*-values for Mantel-Cox three-way comparisons. *p*-values are indicated by the group comparisons made, and the assay number. Pairwise comparisons were run and analyzed if three-way Mantel Cox results indicated statistical significance. A Bonferroni-corrected α value for significance was calculated to compensate for type I errors from comparing multiple groups simultaneously.

Groups Compared	Assay Number	*p*-value[2]
VC40421 vs. MT7907 vs. N2	1	<.0001***
	2	<.0001***
	3	<.0001***
	Collapsed[1]	<.0001***
VC40512 vs. MT7907 vs. N2	1	.0688
	2	<.0001***
	3	.8024
	Collapsed[1]	.0012**
VC40082 vs. MT7907 vs. N2	1	.0107*
	2	.0001***
	3	.0239
	Collapsed[1]	.3108
VC40914 vs. MT7907 vs. N2	1	<.0001***
	2	<.0001***
	3	<.0001***
	Collapsed[1]	<.0001***

*$p \leq .01667$, **$p \leq .0033$, ***$p \leq .00033$, ****$p \leq .000033$

[1] Statistical results for a collapsed data set including data across all three trials.

[2] A Bonferroni-corrected α value of 0.01667 was used as a statistical threshold for significance across all three-way comparisons.

Table A2. Statistical results of Mantel-Cox test for VC40512 test-strain assays. This table reports the *p*-values, hazard ratios, and 95% confidence intervals indicated by comparison made and assay number for the VC40512 test strain assays. The hazard ratio indicates how rapidly worms died in one group compared to another, whereas the confidence interval indicates with 95% certainty that the range of values contains the true mean of the population. A and B groups for hazard ratios are indicated in parenthesis next to *C. elegans* strain names

Groups Compared	Assay Number	Hazard Ratio		95% CI Ratios		*p*-value
		A/B	B/A	A/B	B/A	
VC40512 (A) vs. N2 (B)	1	1.654	0.605	0.826 to 3.313	0.302 to 1.210	.0589
	2	1.046	0.916	0.544 to 2.011	0.497 to 1.837	.8499
	3	0.862	1.160	0.451 to 1.648	0.607 to 2.216	.614
	Collapsed[1]	1.130	0.885	0.771 to 1.657	0.604 to 1.297	.565
VC40512 (A) vs. MT7907 (B)	1	1.684	0.594	0.864 to 3.281	0.305 to 1.157	.0385*
	2	4.271	0.234	1.901 to 9.594	0.104 to 0.526	<.0001****
	3	1.033	0.968	0.542 to 1.968	0.508 to 1.844	.9142
	Collapsed[1]	1.776	0.566	1.184 to 2.635	0.380 to 0.845	.0012**
MT7907 (A) vs. N2 (B)	1	1.075	0.930	0.524 to 2.207	0.453 to 1.909	.8137
	2	0.250	4.001	0.112 to 0.558	1.792 to 8.934	.0001****
	3	0.824	1.214	0.427 to 1.588	0.630 to 2.341	.5185
	Collapsed[1]	0.607	1.647	0.400 to 0.922	1.085 to 2.500	.0063**

*$p \leq .05$, **$p \leq .01$, ***$p \leq .001$, ****$p \leq .0001$

[1] Statistical results for a collapsed data set including data across all three trials.

Table A3. Statistical results of Mantel-Cox test for VC40082 test-strain assays. This table reports the *p*-values, hazard ratios, and 95% confidence intervals indicated by comparison made and assay number for the VC40082 test strain assays. The hazard ratio indicates how rapidly worms died in one group compared to another, whereas the confidence interval indicates with 95% certainty that the range of values contains the true mean of the population. A and B groups for hazard ratios are indicated in parenthesis next to *C. elegans* strain names.

Groups Compared	Assay Number	Hazard Ratio		95% CI Ratios		*p*-value
		A/B	B/A	A/B	B/A	
VC40082 (A) vs. N2 (B)	1	2.61	0.383	1.249 to 5.454	0.183 to 0.801	.0005***
	2	2.402	0.416	1.214 to 4.749	0.211 to 0.823	.0003***
	3	0.497	2.014	0.252 to 0.978	1.022 to 3.969	.0136*
	Collapsed[1]	1.137	0.880	0.779 to 1.658	0.603 to 1.283	.4494
VC40082 (A) vs. MT7907 (B)	1	1.360	0.7354	0.710 to 2.603	0.384 to 1.408	.2236
	2	2.327	0.430	1.176 to 4.604	0.2172 to 0.850	.001***
	3	0.573	1.746	0.284 to 1.100	0.909 to 3.352	.0438*
	Collapsed[1]	1.262	0.793	0.870 to 1.830	0.547 to 1.149	.1631
MT7907 (A) vs. N2 (B)	1	1.615	0.6193	1.823 to 3.167	0.3158 to 1.215	.1002
	2	0.757	1.320	0.393 to 1.459	0.686 to 2.544	.3324
	3	0.755	1.325	0.400 to 1.426	0.701 to 2.503	.2984
	Collapsed[1]	0.882	1.134	0.604 to 1.286	0.777 to 1.655	.4628

*$p \leq .05$, **$p \leq .01$, ***$p \leq .001$, ****$p \leq .0001$

[1] Statistical results for a collapsed data set including data across all three trials.

Table A4. Statistical results of Mantel-Cox test for VC40421 test-strain assays. This table reports the *p*-values, hazard ratios, and 95% confidence intervals indicated by comparison made and assay number for the VC40421 test strain assays. The hazard ratio indicates how rapidly worms died in one group compared to another, whereas the confidence interval indicates with 95% certainty that the range of values contains the true mean of the population. A and B groups for hazard ratios are indicated in parenthesis next to *C. elegans* strain names.

Groups Compared	Assay Number	Hazard Ratio		95% CI Ratios		*p*-value
		A/B	B/A	A/B	B/A	
VC40421 (A) vs. N2 (B)	1	4.054	0.247	1.866 to 8.808	0.114 to 0.536	<.0001****
	2	3.313	0.302	1.620 to 6.775	0.148 to 0.617	<.0001****
	3	2.533	0.395	1.295 to 4.958	0.202 to 0.773	<.0001****
	Collapsed[1]	3.293	0.304	2.172 to 4.992	0.2003 to 0.460	<.0001****
VC40421 (A) vs. MT7907 (B)	1	3.73	0.268	1.749 to 7.957	0.126 to 0.57	<.0001****
	2	3.73	0.268	1.749 to 7.957	0.126 to 0.57	<.0001****
	3	2.964	0.337	1.477 to 5.946	0.168 to 0.677	<.0001****
	Collapsed[1]	3.197	0.313	2.116 to 4.830	0.207 to 0.473	<.0001****
MT7907 (A) vs. N2 (B)	1	2.043	0.489	1.038 to 4.020	0.249 to 0.963	.0033**
	2	0.544	1.839	0.276 to 1.072	0.933 to 3.625	.0276*
	3	0.691	1.446	0.374 to 1.279	0.782 to 2.676	.135
	Collapsed[1]	0.850	1.177	0.589 to 1.226	0.816 to 1.697	.289

*$p \leq .05$, **$p \leq .01$, ***$p \leq .001$, ****$p \leq .0001$

[1] Statistical results for a collapsed data set including data across all three trials.

Table A5. Statistical results of Mantel-Cox test for VC40914 test-strain assays. This table reports the *p*-values, hazard ratios, and 95% confidence intervals indicated by comparison made and assay number for the VC40914 test strain assays. The hazard ratio indicates how rapidly worms died in one group compared to another, whereas the confidence interval indicates with 95% certainty that the range of values contains the true mean of the population. A and B groups for hazard ratios are indicated in parenthesis next to *C. elegans* strain names.

Groups Compared	Assay Number	Hazard Ratio		95% CI Ratios		*p*-value
		A/B	B/A	A/B	B/A	
VC40914 (A) vs. N2 (B)	1	1.307	0.765	0.645 to 2.650	0.377 to 1.550	.3505
	2	0.326	3.070	0.159 to 0.669	1.495 to 6.306	<.0001****
	3	0.231	4.33	0.102 to 0.524	1.908 to 9.827	<.0001****
	Collapsed[1]	0.391	2.555	0.259 to 0.591	1.692 to 3.860	<.0001****
VC40914 (A) vs. MT7907 (B)	1	4.664	0.214	1.861 to 11.690	0.086 to 0.537	<.0001****
	2	1.477	0.677	0.722 to 3.022	0.331 to 1.385	.2497
	3	0.934	1.07	0.510 to 1.711	0.584 to 1.961	.8027
	Collapsed[1]	1.644	0.608	1.102 to 2.454	0.408 to 0.908	.0065**
MT7907 (A) vs. N2 (B)	1	0.265	3.777	0.117 to 0.599	1.670 to 8.540	<.0001****
	2	0.263	3.807	0.124 to 0.558	1.793 to 8.082	<.0001****
	3	0.286	3.497	0.133 to 0.616	1.624 to 7.530	<.0001****
	Collapsed[1]	0.293	3.418	0.188 to 0.455	2.199 to 5.311	<.0001****

*$p \leq .05$, **$p \leq .01$, ***$p \leq .001$, ****$p \leq .0001$

[1] Statistical results for a collapsed data set including data across all three trials.

Appendix B

PCR Products

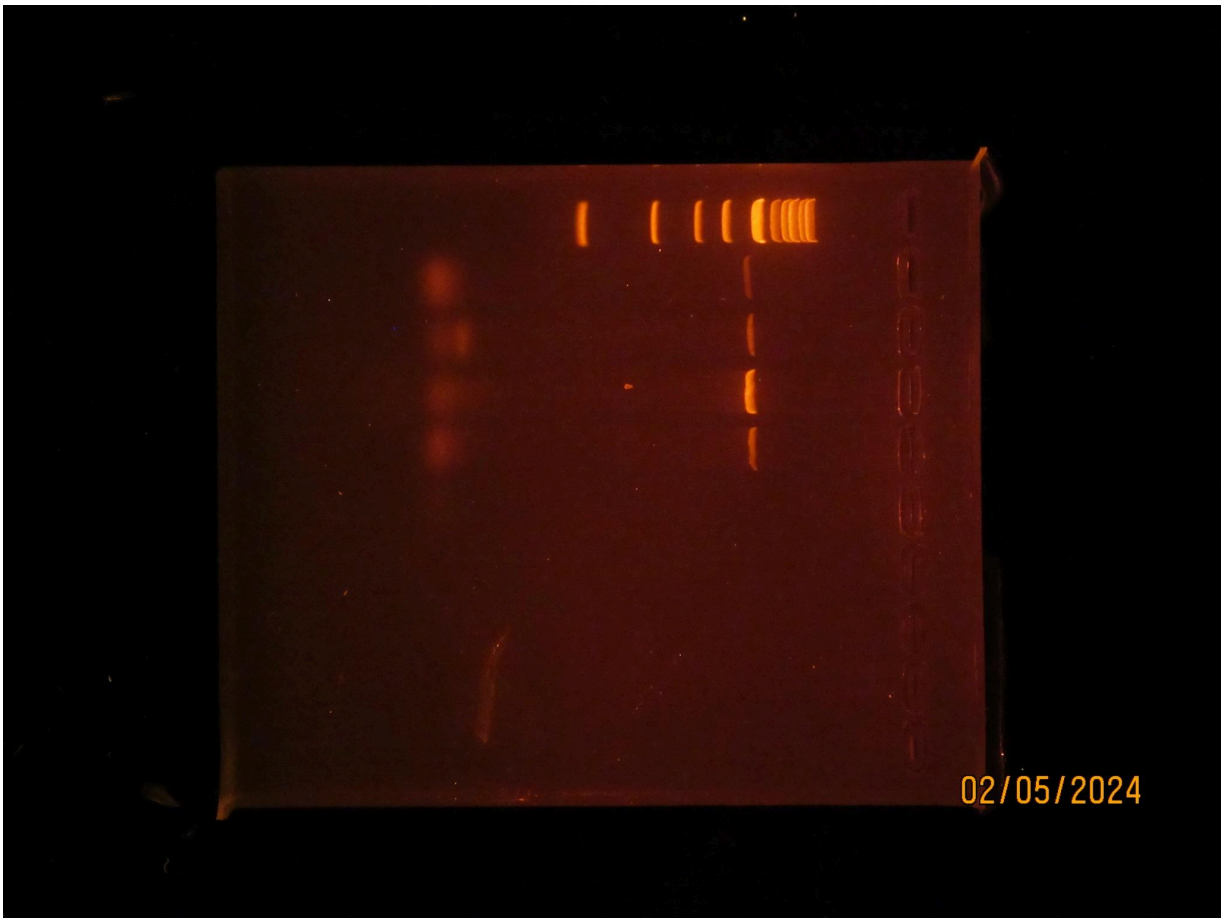

Figure B1. PCR gel electrophoresis products for N2, MT7907, VC40082, and VC40914. PCR experiments and gel electrophoresis were performed in order to verify that each strain assayed contained mutations in the *vha-12* gene of interest. We observed positive PCR products for all N2, MT7907, VC40914, and VC40082, which can be visualized above. Lane assignments are as follows: Lane 1: 1kb DNA ladder, Lane 2: N2, Lane 3: MT7907, Lane 4: VC40914, Lane 5: VC40082, Lane 6: negative control (note: photograph of gel displayed sideways).

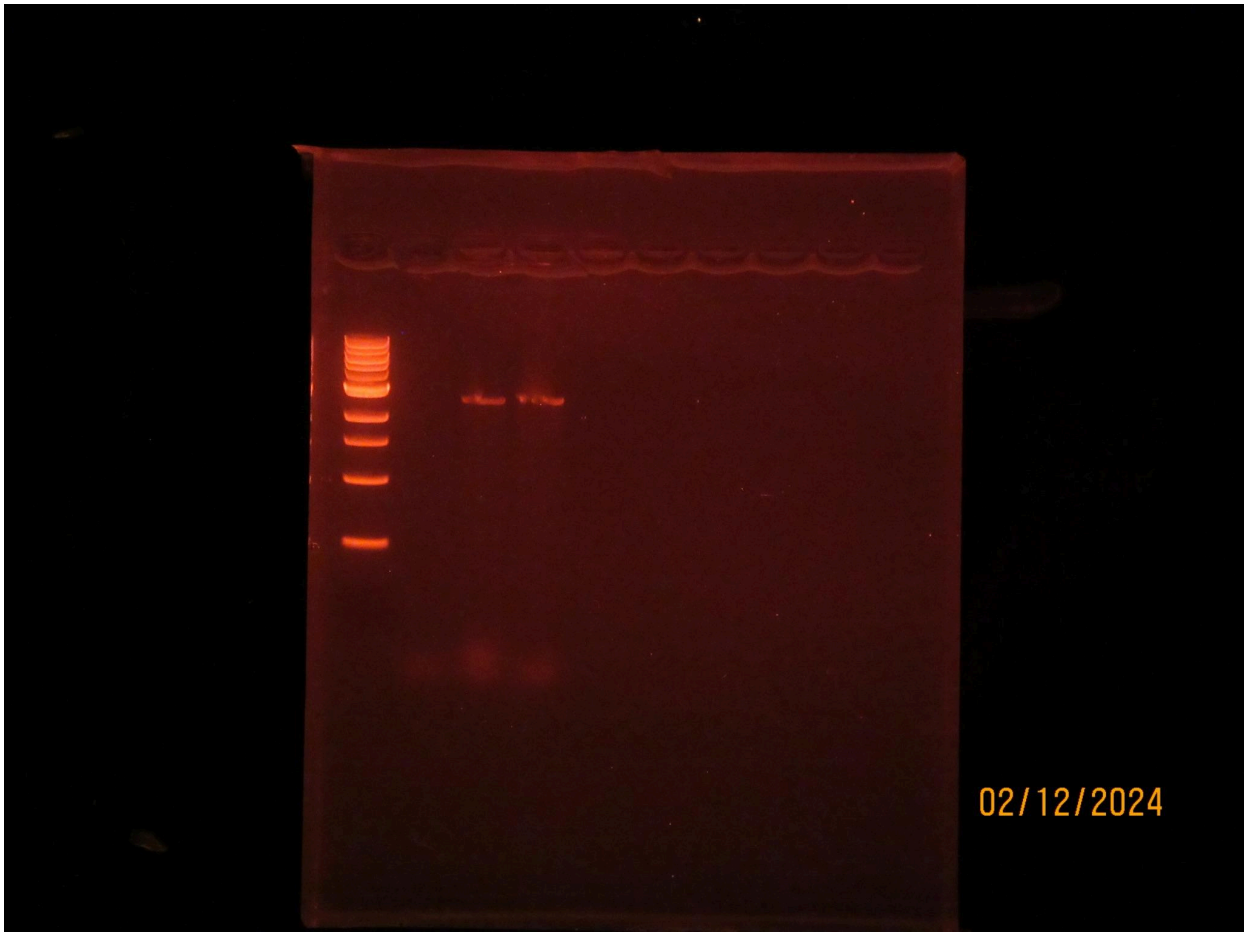

Figure B2. PCR gel electrophoresis products for VC40512 and VC40421. PCR experiments and gel electrophoresis were performed in order to verify that each strain assayed contained mutations in the *vha-12* gene of interest. We observed positive PCR products for both VC40512 and VC40421, which can be visualized above. Lane assignments are as follows: Lane 1: 1kb DNA ladder, Lane 2: negative control, Lane 3: VC40512, Lane 4: VC40421

Appendix C

Supplemental Body-Bending Results

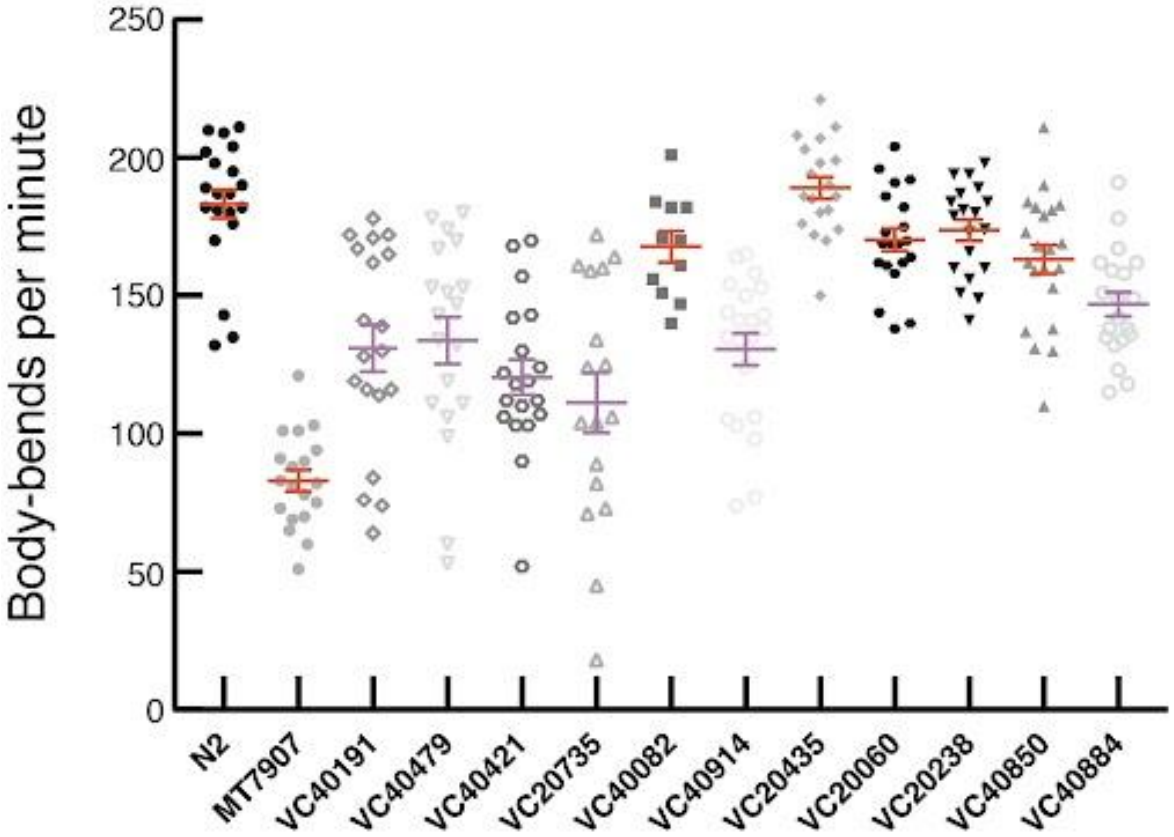

Figure 1C. Body-bending results indicate VC40421 and VC40914 exhibit locomotion defects compared to wild-type. The figure above (adapted from Dorjey Sherpa) shows the number of body-bends per minute (y-axis) for different *C. elegans* strains (x-axis) containing allelic variations of the *vha-12* gene. Worms were suspended in water and their average number of body-bends were recorded. Decreases in body bends correspond to locomotion defects associated with changes in synaptic transmission. The known aldicarb resistant mutant, MT7907, exhibits the most significant decrease in body-bends per minute compared to wild-type (N2), closely followed by aldicarb hypersensitive mutant, VC40421, and another identified aldicarb resistant mutant, VC40914. Alternatively, the VC40082 strain exhibits no significant difference in the number of body-bends per minute compared to wild-type.

Appendix D

VHA-12 Sequence Alignment

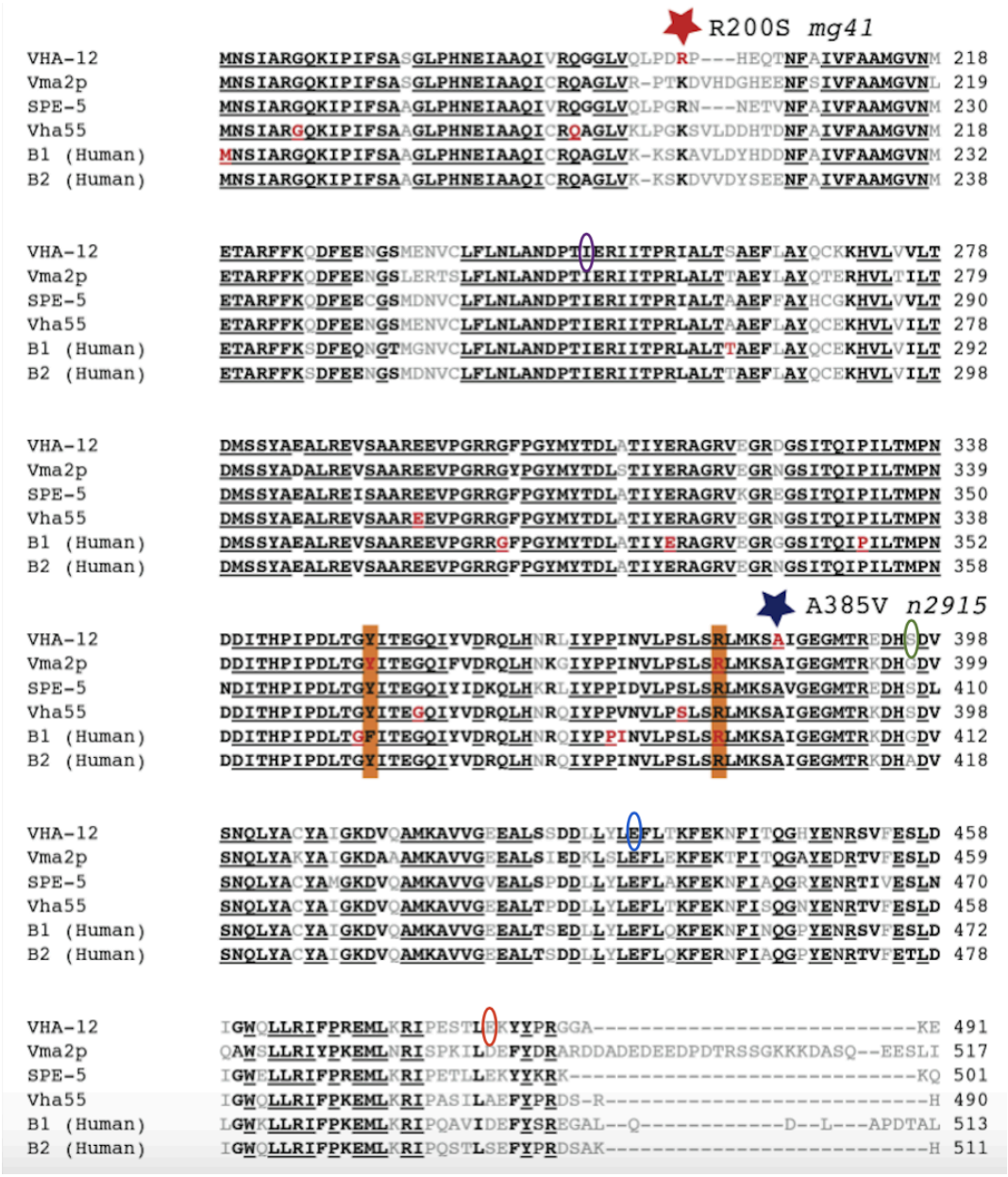

Figure 1D. Amino acid sequence alignment of VHA-12. Amino acid mutations for VC40512 (E433K, circled in blue), VC40082 (S296F, circled in green), VC40421 (I249L, circled in purple), and VC40914 (E481K, circled in red) were identified using the amino acid sequence alignment of the VHA-12 polypeptide, adapted from Ernstrom et al. 2012. Highly conserved catalytic tyrosine (Y) and arginine (R) residues are highlighted in orange.